Ore Geology Reviews 88 (2017) 352–369

Contents lists available at ScienceDirect

Ore Geology Reviews

journal homepage: www.elsevier.com/locate/oregeo

Integrated field, mineralogical and geochemical characteristics of Caçapava do Sul alvikite and beforsite intrusions: A new Ediacaran carbonatite complex in southernmost Brazil

Tiara Cerva-Alves [a,*], Marcus Vinicius Dorneles Remus [a], Norberto Dani [a], Miguel Angelo Stipp Basei [b]

[a] Instituto de Geociências, Universidade Federal do Rio Grande do Sul, Avenida Bento Gonçalves, 9500, 91501-970 Porto Alegre, Rio Grande do Sul, Brazil
[b] CPGeo, Instituto de Geociências, Universidade de São Paulo, Rua do Lago 562 Cidade Universitária, 05508-080 São Paulo, Brazil

ARTICLE INFO

Article history:
Received 6 January 2017
Accepted 16 May 2017
Available online 19 May 2017

Keywords:
Carbonatite
Alvikite
Beforsite
Caçapava do Sul
Geochemistry
Geochronology

ABSTRACT

The integrated evaluation of soil geochemistry, aerogammaspectrometry (eTh), geological and structural mapping associated with the description of boreholes and outcrops in the Caçapava do Sul region, southernmost Brazil, led to the discovery of two carbonatite bodies. They are located near the eastern and southeastern border of Caçapava do Sul Granite and intrude the Passo Feio Complex. The carbonatite system is composed of early pink-colored alvikite followed by late white beforsite dikes. The carbonatites are tabular bodies concordant with the deformed host rocks. Petrographic and scanning electron microscopy show that the alvikites are dominantly composed of calcite with subordinate apatite, magnetite, ilmenite, biotite, baddeleyite, zircon, rutile, pyrochlore-like and rare earth element minerals. Beforsite is composed of dolomite and has the same minor and accessory minerals as the alvikite. U-Pb zircon geochronology via laser ablation inductively coupled plasma mass spectrometry (LA-ICP-MS) was performed on a beforsite sample, yielding a 603.2 ± 4.5 Ma crystallization age. The carbonatite was emplaced an Ediacaran post-collisional environment with transpressive tectonism and volcanic activity marked by shoshonitic affinity.

1. Introduction

The study of carbonatites is relevant from both economic and scientific viewpoints. Carbonatites can be important sources of economically strategic mineral deposits of Nb, U, Th, Ti, Ba, Sr, rare earth elements (REE) and industrial minerals such as apatite and magnetite (Hogarth, 1989; Mariano, 1989). These special rocks originate in the mantle, but many details about their genesis are under debate. According to Jones et al. (2013, and references therein), the accepted theories for the carbonatite origin include "(1) residual melt of fractionated carbonated nepheline or melilite; (2) immiscible melt fractions of CO_2-saturated silicate melts and (3) primary mantle melts generated through partial melting of CO_2-bearing peridotite".

Usually carbonatites occur in relatively small intrusive plugs, dikes, sills, breccias, veins or as composite plutonic ring complexes in association with a diversity of alkaline silicate rocks such as nephelinites, phonolites, nephelite syenites, ijolites, urtites, melilitolites, pyroxenites, peridotites, kimberlites and lamprophyres (Barker, 1989; Woolley and Kempe, 1989; Winter, 2010). They can also occur without associated coeval silicate rocks. In this case, these carbonatites tend to be rich in dolomite (Woolley, 2003; Winter, 2010; Hammouda and Keshav, 2015).

In southernmost Brazil, four carbonatite intrusions were discovered by Companhia Brasileira do Cobre – CBC, Geological Survey of Brazil – CPRM and Mining Ventures Brasil Group – MVB (Parisi et al., 2010; Toniolo et al., 2010; Grazia et al., 2011; Rocha et al., 2013). The ages of the carbonatites remain undetermined. The Três Estradas body was the first carbonatite discovered by a consultant geologist of the Companhia Brasileira do Cobre from borehole chemical and petrographical data during the development of a gold project. The Joca Tavares carbonatite was found by the Geological Survey of Brazil – CPRM through aerogammaspectrometry and field examination. The Caçapava do Sul carbonatites, main targets of this work, comprise two reported occurrences called Picada dos Tocos and Passo Feio, and were discovered by follow-up of geochemical anomalies from a soil survey by Mining Ventures Brasil Group.

The Caçapava do Sul carbonatites are a recent discovery, so a description of the field relationships, petrography, geochemistry and age of the bodies is required. The techniques used include

* Corresponding author.
E-mail address: tiara.geologia@gmail.com (T. Cerva-Alves).

http://dx.doi.org/10.1016/j.oregeorev.2017.05.017
0169-1368/

geological mapping of the carbonatites, analyses of drill cores and outcrop samples using petrographic conventional microscopy and scanning electron microscope techniques. Total rock chemical analyses for major and trace elements using inductively coupled plasma mass spectrometry (ICP-MS) and inductively coupled plasma atomic emission spectrometry (ICP-AES) are also additional techniques. Zircon crystals were dated with laser ablation inductively coupled plasma-mass spectrometry (LA-ICP-MS). The interpretation of the data led to the conclusion that the carbonatites originated in the mantle in a sequence of at least two events, starting with an alvikite intrusion into Neoproterozoic host rocks followed by a beforsite intrusion at ca. 603.2 ± 4.5 Ma. The multi-analytical approach led to the description of these carbonatite bodies.

2. Geological context

The Brazilian Shield (Fig. 1) includes Archean and Proterozoic cratons and Brasiliano/Pan-African mobile belts covered by Phanerozoic sedimentary basins (Almeida, 1967; Almeida et al., 1981; Cordani and Brito-Neves, 1982; CPRM, 2015). Archean to Early Proterozoic rocks are found in the large Amazonian and São Francisco cratons as well as in the smaller Rio de La Plata, São Luís and Luiz Alves cratonic fragments (Fuck et al., 2008).

From Late Neoproterozoic to Early Cretaceous, the central-southeastern part of the Brazilian Shield was within Gondwanaland (Riccomini et al., 2005; Veevers, 2007), which is represented by the Mantiqueira orogenic system, comprising the belts Dom Feliciano (Uruguay and southern Brazil), Ribeira (Paraná, São Paulo, Minas Gerais and Rio de Janeiro states) and Araçuaí (Espírito Santo, eastern Minas Gerais and southern Bahia states). The Dom Feliciano belt developed during three major events: (1) crustal accretion phase with juvenile magmatism between ca. 900–850 Ma, (2) continental arc magmatism and accretion between 770–680 Ma, and (3) collisional event including metamorphism between 650–620 Ma and a main magmatic phase between ca. 650–550 Ma, with intense crustal anatexis (Saalmann et al., 2010; Philipp et al., 2016). Tectonic reactivations along shear zones and other disconti-

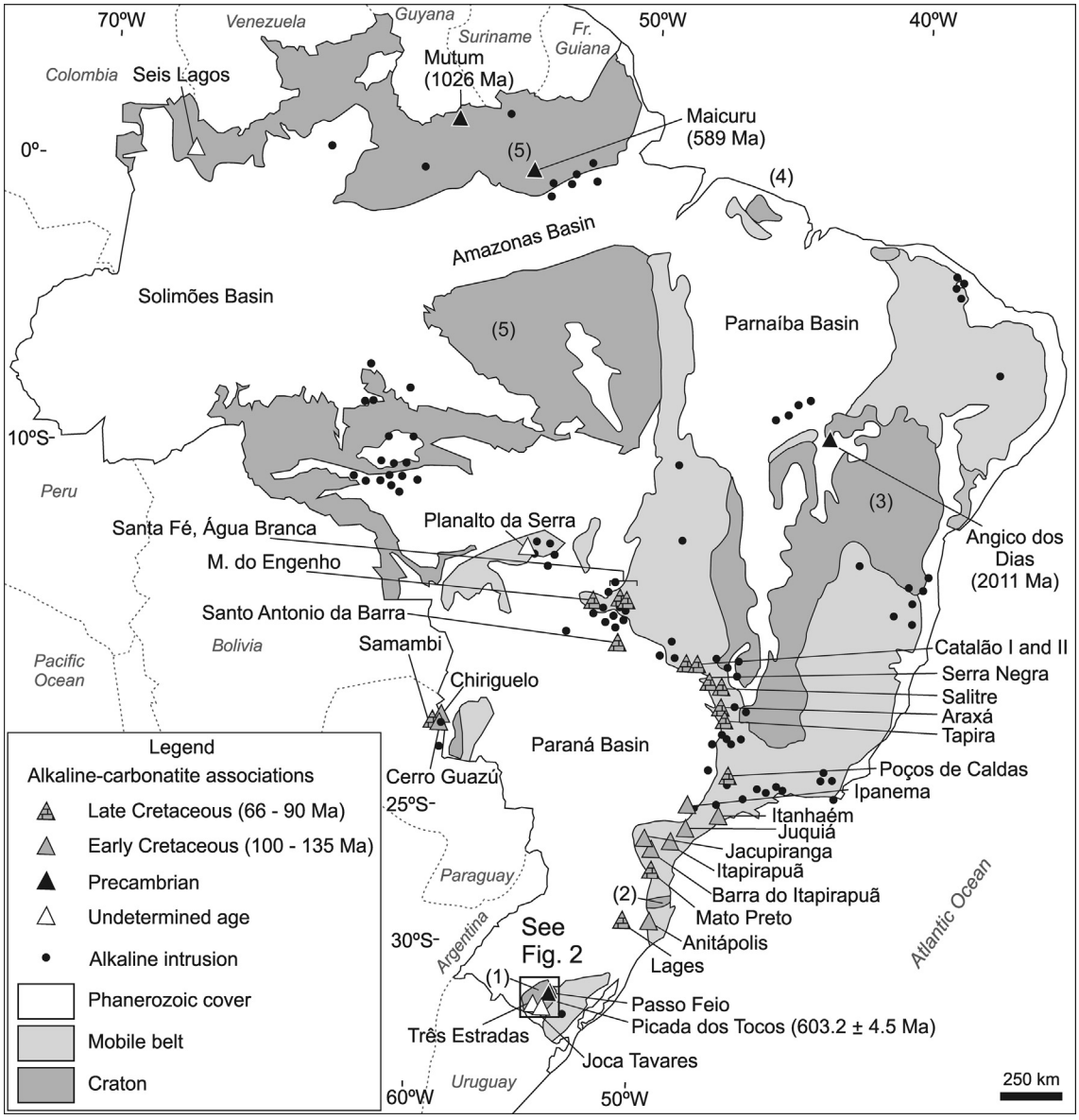

Fig. 1. Carbonatite and alkaline rock occurrences in Brazil, including the presently described bodies. (1) Rio de La Plata Craton, (2) Luiz Alves Craton, (3) São Francisco Craton, (4) São Luís Craton, (5) Amazonas Craton. Modified from Issler et al. (1975), Silva et al. (1988), Alkmin (2004), Giovanini (2013), CPRM (2015).

nuities in the basement rocks played a major role in the distribution of magmatic activity (Riccomini et al., 2005).

Many types of alkaline and alkaline-carbonatitic complexes with different ages are widespread in the southern region in Brazil in association with flexure and fractured zones (Biondi, 2005). Angico dos Dias, Mutum and Maicuru are examples (Fig. 1) of rare Precambrian carbonatite occurrences in Brazil (Lemos and Costa, 1987; Gomes et al., 1990; Costa et al., 1991; Angélica and Costa, 1993; Lapin et al., 1999; Antonini et al., 2003). The main known economic carbonatite complexes and associated alkaline rocks occur from the Permian-Triassic to Paleogene along mobile belts (Brasiliano Cycle) and at the Paraná Basin borders (Riccomini et al., 2005; Gomes and Comin-Chiaramonti, 2005).

In southernmost Brazil, alkaline silicate rocks are represented by syenites, phonolites, kimberlites, lamprophyres and picrites that are located in the central-eastern area of the Sul-Riograndense Shield. These rocks intrude both the Phanerozoic cover around the Paraná volcanic province and the Precambrian basement (Burger et al., 1988; Svisero and Chieregati, 1991; Tedesco and Robaina, 1991; Caldasso and Sander, 1994; Philipp et al., 2006; Adrião, 2015). Late- to post-collisional magmas, including saturated alkaline magmatism (syenites) to supersaturated (granitoids and alkaline gneiss), are dated at 610–560 Ma (Silva et al., 2005; Bitencourt et al., 2015), and isolated alkaline rocks (A-type granite to syenogranite) range in age from 613 Ma to 549 Ma (Veevers, 2007 and references therein). Volcanic and plutonic rocks with shoshonitic affinity and sodic alkaline silica saturated were formed in the interval of 600–587 Ma (Liz et al., 2005; Sommer et al., 2006; Gastal et al., 2006).

The four recently-discovered carbonatite bodies occur near second (and third) order fractures oriented NW and NE (Fig. 2), in three distinct geotectonic compartments: (1) Três Estradas carbonatite, intrusive into 2.5–2.1 Ga granulitic and amphibolitic rocks from the Rio de La Plata Craton, (2) Passo Feio and Picada dos Tocos occurrences in Caçapava do Sul, intrusive into Neoproterozoic metamorphic rocks from the Passo Feio Complex, Dom Feliciano Belt, interpreted as island arc and continental margin, and (3) Joca Tavares body in an intracontinental rift context, intruding fluvial and eolian Cambrian sediments from the Guaritas Group, Camaquã post-collisional Basin (Rocha et al., 2013; Toniolo et al., 2013; Maciel, 2016). No contemporaneous silicate alkaline rocks are described in association with the carbonatite occurrence.

The Caçapava do Sul region is part of the São Gabriel Terrain (Chemale, 2000), a mantle-derived juvenile section of the extensive Brasiliano Orogen of South America. The Terrain is delimited by two principal structures: the NW-trending transpressive Ibaré shear zone in the south/southwest and the Caçapava shear zone in the east/southeast (Silva et al., 2005). The origin of Neoproterozoic rock associations of the São Gabriel Terrain is related to an arc system (Remus et al., 1999; Hartmann et al., 2000) formed during the early evolution of the Dom Feliciano Belt, as a result of plate convergence and closure of the Adamastor Ocean (Lopes et al., 2015; Philipp et al., 2016).

The Passo Feio Complex (Ribeiro et al., 1966; Bitencourt, 1983; Remus et al., 2000) hosts the Caçapava do Sul carbonatites and comprises mainly metasedimentary rocks (slate, phyllite, mica schist, marble, quartzite, gneiss, and calc-silicate) and orthoderived rocks (amphibolite, talc/tremolite schist and metavolcanic/metavol

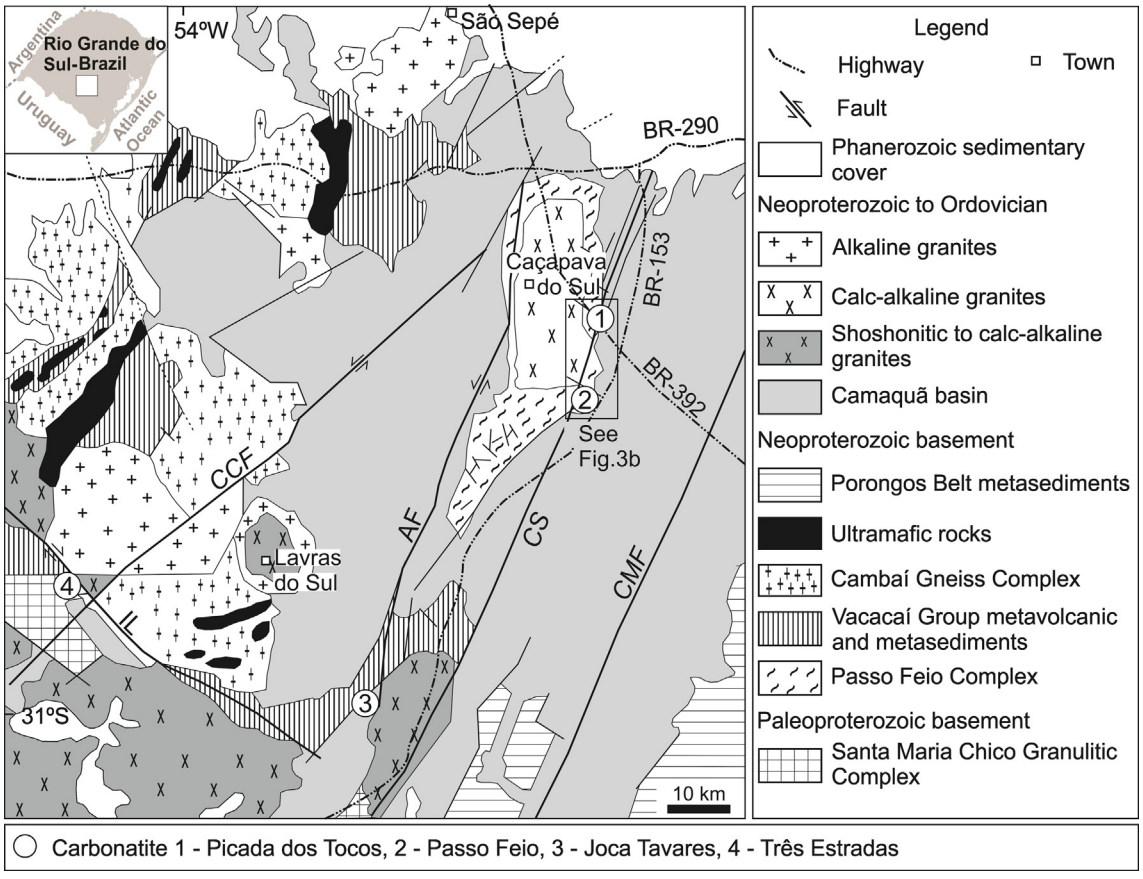

Fig. 2. Geological units of the São Gabriel Terrain, Precambrian Sul-Riograndense Shield, southern Brazil, showing the main geotectonic units and carbonatite bodies. CCF = Cerro dos Cabritos fault zone, AF = Andrade fault zone, CMF = Camaquã Mine fault zone, CS = Caçapava shear zone, IL = Ibaré lineament. Modified from Remus et al. (2000).

canoclastics rocks). Regional metamorphism varies from greenschist facies – chlorite zone to amphibolite facies – staurolite zone (Hartmann et al., 1990; Hartmann and Remus, 2000; Remus et al., 2000). The presence of an old crust (Archean) and the generation of a retroarc continental basin around 760–780 Ma was dated by zircon U-Pb SHRIMP analyses from Passo Feio metasediments (Remus et al., 2000). The closure of this basin and the initial deformation of the rock sequence (M1 and D1) started at 700 Ma. M2 metamorphism and D2 deformation are related with the Caçapava do Sul granite syntectonic intrusion at approximately 562 Ma (Bitencourt, 1983; Remus et al., 2000). The sequence has centripetal structure dipping 20°, exposed around the Caçapava do Sul granite, contemporaneous with the NE strike-slip related fault system that overprints the Bom Jardim Group, a volcanosedimentar Ediacaran unit from the Camaquã Basin. Field evidence indicates that the Caçapava do Sul carbonatites were subjected to the same deformation events of the associated Ediacaran country rocks, making significant the dating of the carbonatite.

3. Local geology

We discuss the main geological controls of the two carbonatite bodies, including size and geometry, internal structures, mineral assemblage and host rock contact relationships. The study areas (Fig. 3) are underlain by the Precambrian Passo Feio Complex, controlled by NW, NE and N-S fault systems. The N-S normal fault from the Picada dos Tocos occurrence defines the tectonic contact between the Passo Feio Complex and the younger Bom Jardim Group (Remus et al., 1999; Paim et al., 2000).

Several carbonatite dikes and sill-like intrusions are parallel to the bedding and schistosity (So/S1) of the metasedimentary host rocks. In the Picada dos Tocos occurrence, the carbonatite bodies follow a major NS-trending fault while in the Passo Feio occurrence, the carbonatites are controlled by NE-NW faults.

The Picada dos Tocos bodies (Fig. 3c) constitute a 2.2 km long and ca. 80 m wide tabular unit, dipping to the southeast (N110°/40° to 60°), concordant with the host rock schistosity and

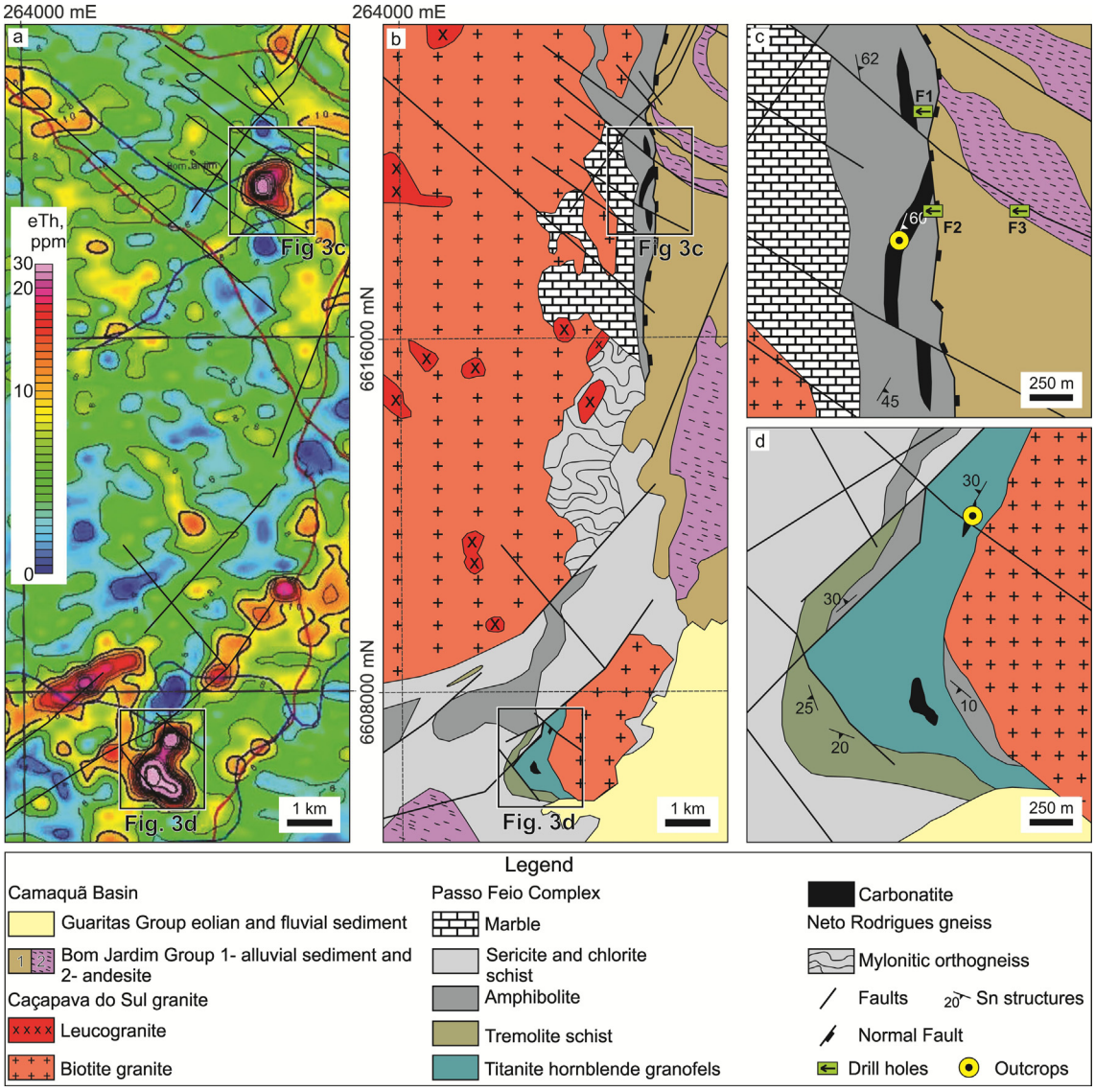

Fig. 3. (a) Radiometric contour map of Th in ppm (CPRM, 2010); (b) geological map of the Caçapava do Sul region, including (c) Picada dos Tocos and (d) Passo Feio bodies, showing bedding, foliation, outcrops and sampled drill cores. Map coordinates are in UTM (m), Datum SAD69, Zone 22S.

folds (Rocha et al., 2013). The drilling campaign conducted by Mining Ventures Brasil Group confirmed a carbonatite system from the surface to at least 290 m depth. In the northwest, transcurrent ruptile faults imprinted 100 m sinistral displacement in the body. The carbonatite comprises an early pink alvikite and a later white beforsite phase with centimeter to meter sizes. They form dikes/veins that are interleaved and concordant with thick to thin mafic layers. The alvikite has mainly calcite with accessory apatite, magnetite, ilmenite, rutile, zircon, baddeleyite, barite, thorite, pyrochlore-like and rare earth element (REE) minerals. Pyrite, chalcopyrite, chlorite, quartz and biotite are also present in different proportions. The beforsite was identified only in drill cores and has around 80 vol.% dolomite, with the same minor and accessory minerals as the alvikite. Variation within the carbonatite system was defined from drill core samples, with the carbonatite showing different degrees of hydrotermal alteration, contact relationships (including sharp and gradational), grain size and recrystalization. The identified REE-bearing phases include fine-grained monazite, pyrochlore-like minerals rich in Nb, Th and REE, bastnaesite and allanite.

The Passo Feio carbonatite has limited outcrop exposure; no drilling is available (Fig. 3d). Abundant titanite-hornblende granofels occurs associated with the carbonatite body with similar geophysical signature to the Picada dos Tocos occurrence. A small alvikite outcrop in the north of this area shows a banded rock with layers of abundant calcite, apatite, ilmenite and magnetite intergrowth, with enriched layers of tremolite, and structures suggest the presence of a body dipping 30° NW. A second alvikite occurrence was defined from float samples and heavy mineral trace abundance in soil (mainly apatite and monazite).

Thick mafic lenses between the layers of carbonatites are composed of biotite and amphibole (actinolite, hornblende and cummingtonite), with relics of diopside, in a matrix comprised of calcite, magnetite, ilmenite, rutile, apatite and pyrite. Carbonatites and mafic bands were strongly deformed, metasomatized and affected by hydrothermal fluids, as shown by stockworks and with veins of calcite, chlorite, hematite, chalcopyrite/pyrite and quartz, frequently close to NW faults. Some macroscopic relationships among these mineral phase are shown in Fig. 4.

As noted in drill cores, hydrothermally-altered rocks were subjected to carbonation of the matrix and display increase of apatite and magnetite minerals caused by the carbonatite intrusion. This process is restricted to the envelope of Passo Feio amphibolites. At the top, the brecciated contact of the hydrothermally-altered rocks with pelites and sandstones from the Camaquã Basin occurs abruptly, without evidence of hydrothermal activity. The basal transitional zone is marked by bands with grossular in the host rock, with decrease of carbonates, magnetite and apatite minerals in the matrix.

In the Passo Feio occurrence, the host rocks are homogeneous, green-colored, with phaneritic texture which is usually medium-grained, occasionally coarse-grained, and locally porphyritic with centimetric megacrysts of titanite. Close to the contact, there is a garnet-titanite hornblende granofels rich in albite, caused by a sodic fenitization).

The local geology indicates therefore that the geometry of the carbonatite bodies is controlled by the type, permeability and density of host rock and tectonism. The fine grain size suggests that the studied carbonatite bodies are a shallow intrusion.

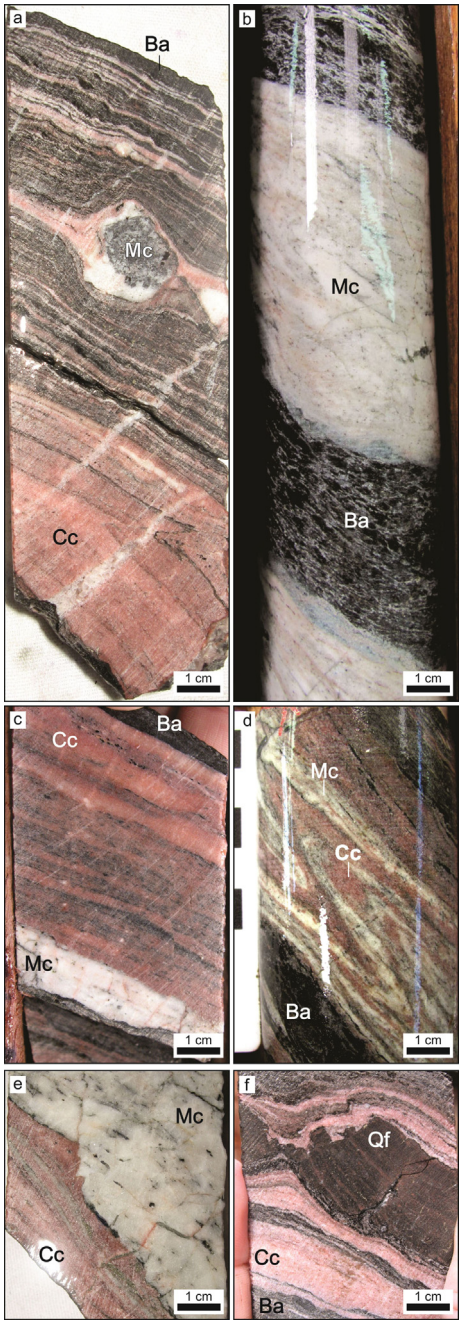

Fig. 4. Diamond drill cores showing (a) bands of pink alvikite interbedded with dark biotite amphibolite, with a globular beforsite xenolith; (b) beforsite and coarse biotite amphibolite interval; (c) foliated biotite amphibolite and pink alvikite, and white beforsite vein showing abrupt concordant contact; (d) interbedded and folded white beforsite and pink alvikite; (e) abrupt concordant contact between beforsite and alvikite; (f) dark biotite amphibolite and pink alvikite interbedded with a quartz-feldspathic fragment. Ba – biotite amphibolite, Cc – alvikite, Mc – beforsite, Qf – quartz-feldspar xenolith rock.

4. Materials and methods

The varied methodology used included satellite images, aerial photographs, aerogammaspectrometry (eTh), geological and structural mapping associated with the description of drill cores and outcrops. The petrographic analysis and scanning electron microscopy were made on 31 thin sections. Major and trace elements of 21 whole-rock samples were analyzed at ALS Minerals (Belo Horizonte, Minas Gerais, Brazil). The analytical program at ALS comprised inductively coupled plasma atomic emission spectrometry (ICP-AES) analyses for major and trace elements, and inductive coupled plasma techniques (ICP-MS) for REE determinations. Eight zircon crystals were separated from a zirconium-rich borehole sample, and were studied using LA-ICP-MS geochronology at the Universidade de São Paulo.

The investigated samples are mainly from drill cores provided by Mining Ventures Brasil Group, and part of a geochemical exploration program at Picada dos Tocos occurrence. Surface samples were collected at both Picada dos Tocos and Passo Feio intrusions. In spite of the small area covered, the available samples are considered representative of the carbonatites and host rocks.

Petrography was carried out at the Instituto de Geociências (IGeo), Universidade Federal do Rio Grande do Sul (UFRGS), using a LEICA optical microscopy, model DM4500, in transmitted polarized and reflected light to identify the major constituent minerals and textural characteristics. Minerals with small size or intimate association with other minerals were studied with a ZEISS EVO MA10 conventional scanning electron microscope fitted with tungsten filament, operating at voltages of 0.2–20 kV. The ZEISS microscope is equipped with a secondary electron detector camera; a backscattered electron detector (BSE) coupled with energy dispersive X-ray spectrometry detector (EDS); and calibrated with natural and synthetic standards. More than 2000 points were analyzed.

Geochemical and petrographical data help to determine zircon abundance and quality, so one sample of beforsite was selected for the characterization of the carbonatite age (sample TA-19). Alvikite zircons were discarded because they are too small for dating, and because of the high possibility of contamination from the host rock. Beforsite zircon grains were concentrated from one drill core sample with 1460 ppm Zr; the presence of zircon was confirmed in thin sections. Because of the small volume of rock available, the sample was totally dissolved in HCl 100% solution to eliminate the carbonate matrix. Heavy minerals were separated by conventional procedures, including isodynamic Frantz magnetic separator and heavy liquid as Bromoform and Diiodomethane, and the final selection was carried out by hand picking. Zircons were mounted in epoxy resin, polished using diamond paste to expose their inner parts. Sample preparation was made at IGeo laboratories. Imaging was made by backscattered electrons (BSE) to determine the internal structures of zircon. Only clear zircon grains free of imperfections, fractures and mineral inclusions were selected for isotopic analyses.

U-Pb isotopic compositions were performed with a laser ablation inductively coupled plasma-mass spectrometry (LA-ICP-MS) at Universidade de São Paulo, Brazil. The equipment includes a New Wave UP-213A/F, with a laser ablation sampler coupled to a mass spectrometer with quadrupole analyzer, working with Nd-YAG laser in the 193 nm wavelength. The powder of the output beam is maximum (7 mJ/pulse) for a 6 Hz reception rate of pulse, and the crater size is about 30 μm. Each sample and standard was ablated for 40 s of data acquisition. The analytical methods, limits of detection, operational parameters, forms of data processing, accuracy, precision and other details of the technique,

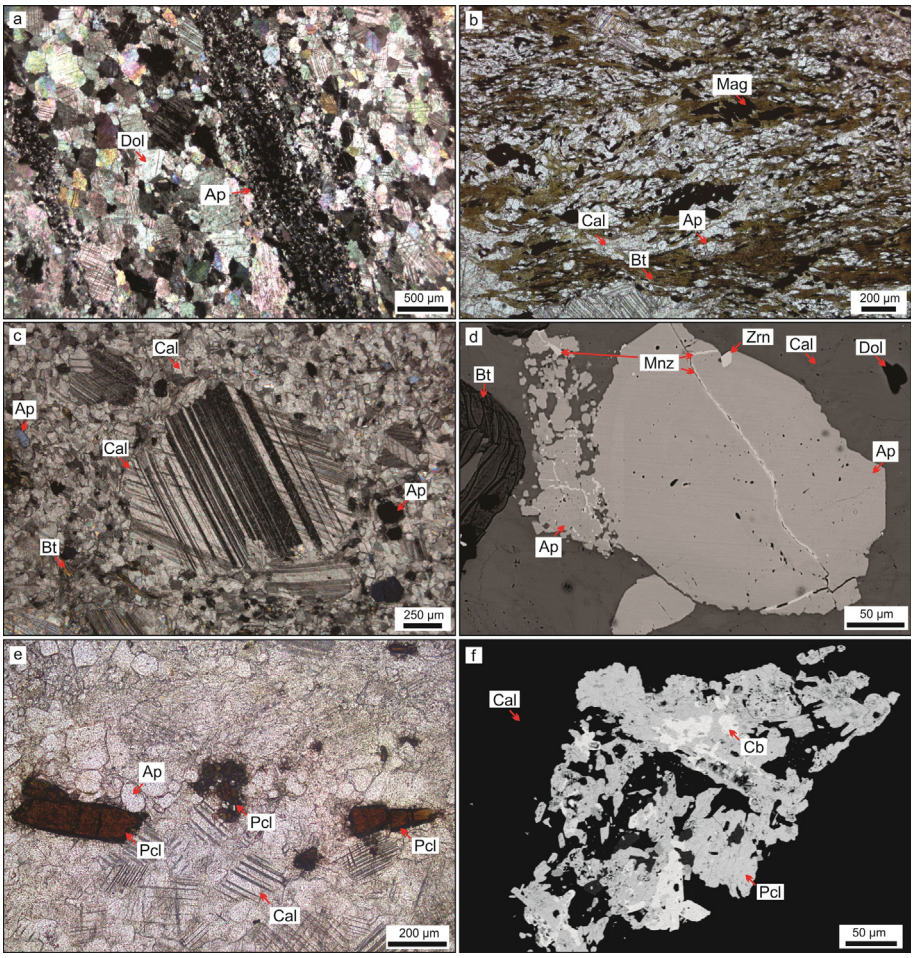

Fig. 5. Selected textural characteristics of Passo Feio and Picada dos Tocos carbonatites: (a) beforsite showing dolomitic matrix and levels with apatite concentration in cross-polarized light (XPL); (b) mylonitic calc-silicate band with aligned biotite, magnetite and apatite grains, all affected by intense carbonation in plane-polarized light (PPL); (c) carbonate phenocryst in a carbonate matrix, showing mortar texture (XPL); (d) apatite showing zircon inclusion and cracks filled with monazite in backscattered electron images (BSE); (e) euhedral crystals of thorium-rich pyrochlore-like minerals from alvikite sample (PPL); (f) fragmented pyrochlore-like minerals associated with ferrocolumbite in a calcite matrix (BSE). Ap – apatite, Bt – biotite, Cb – ferrocolumbite, Dol – dolomite, Mag – magnetite, Mnz – monazite, Pcl – pyrochlore-like mineral, Zrn – zircon.

instrumentation and procedures of this equipment are described in Andrade et al. (2014).

The use of these integrated techniques resulted in the discovery of the Caçapava do Sul carbonatites and their characterization. Significant results were obtained from each analytical technique.

5. Results

5.1. Petrography and mineral chemistry

Field relationships between beforsite and alvikite are complex and their contacts in outcrops and drill cores are variable. The carbonatite system and host rocks show evidence of post-magmatic tectonic events related to ductile-brittle tectonism, including folding, brecciation, recrystallization and grain-boundary migration and intergranular foliation with alignment of elongate carbonate, apatite and biotite crystals. Some domains of carbonatite bodies show consistent veinlet patterns cross cutting foliation, filled by calcite and chlorite (generation 1), quartz and chlorite (generation 2), pervasive pyrite and chalcopyrite and fracture filling (generation 3) and hematite fracture filling (generation 4).

Zones with minerals resistant to ductile deformation contain grains of mechanically-twinned calcite, dolomite and biotite with some bent cleavage. Considering the textural and compositional aspects observed in the hand specimens, thin sections and BSE imaging, these rocks can be considered as metacarbonatites.

5.1.1. Carbonatites

Calcite and dolomite are the dominant minerals in the Picada dos Tocos and Passo Feio carbonatites, and constitute up to 80 vol.% of the rock. Biotite xenocrysts and hydrothermally-altered xenoliths of the biotite amphibolitic host rocks are abundant.

The beforsite layers are fine-grained and typically exhibit an inequigranular banded structure due to the discontinuously aligned layers, laminae and lenses of elongate apatite crystals. They also contain minor, but variable proportions of ilmenite, magnetite, zircon, baddeleyite, REE and Nb minerals sandwiched between dolomite grains (Fig. 5a).

The alvikite portion displays banding, evidenced by elongated calcite aggregates, biotite and apatite. The rock is also strongly marked by millimetric actinolite-biotite-chlorite mylonitic calc-silicate bands, possibly host rock xenoliths, affected by intense carbonation (Fig. 5b). Both carbonatite types have similar accessory minerals and grain size. Their contacts are abrupt and concordant, locally diffuse.

Calcite and dolomite are anhedral with straight or serrated boundaries, ranging in size from a few tens of micrometers to up

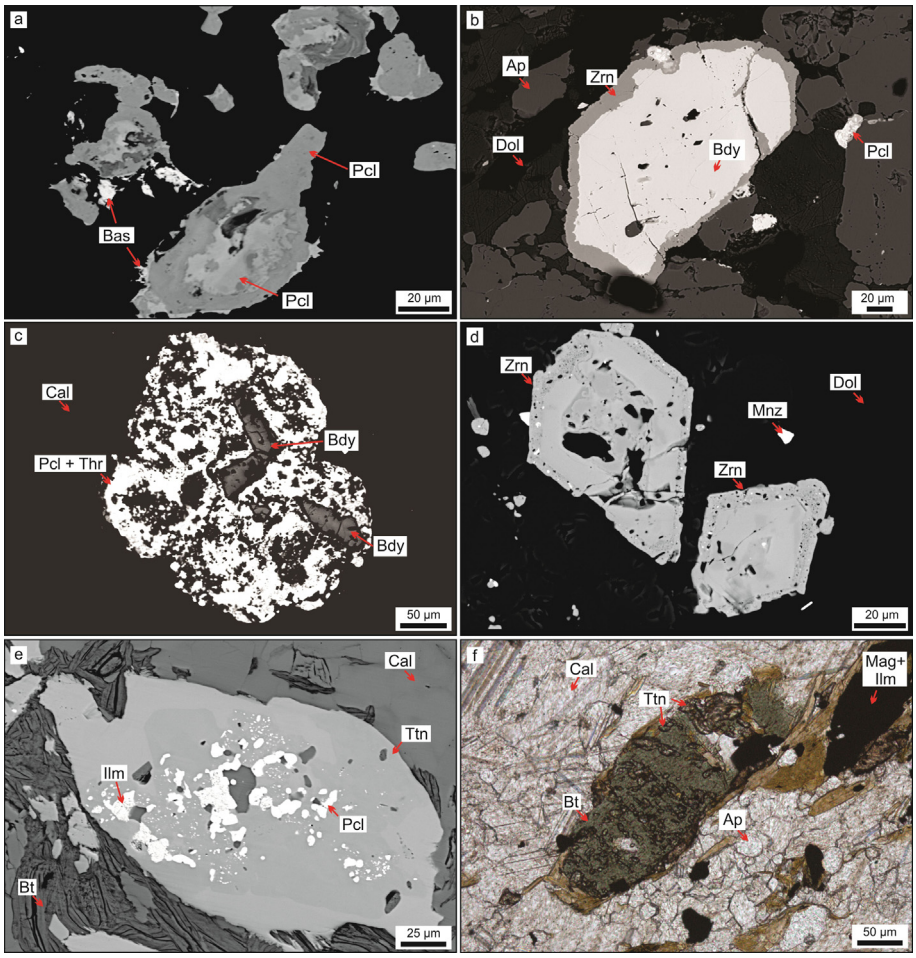

Fig. 6. Selected textural characteristics of Passo Feio and Picada dos Tocos carbonatites: (a) pyrochlore-like minerals with oscillatory composition altered to bastnaesite in backscattered electron images (BSE); (b) baddeleyite grain with zircon overgrowth (BSE); (c) baddeleyite inclusions in pyrochlore and thorite aggregates (BSE); (d) zoned bipyramidal zircon crystals and monazite dispersed in a dolomitic matrix (BSE), dated sample TA-19; (e) pyrochlore-like minerals and ilmenite inclusions in zoned titanite with subtle variable Fe content associated with biotite (BSE); (f) biotite grains substituted by titanite, magnetite and ilmenite in a matrix composed of calcite and apatite in plane-polarized light (PPL). Ap – apatite, Bdy – baddeleyite, Bt – biotite, Cal – calcite, Dol – dolomite, Ilm – ilmenite, Mag – magnetite, Mnz – monazite, Pcl – pyrochlore-like mineral, Thr – thorite, Ttn – titanite, Zrn – zircon.

to 2 mm. They may also be porphyritic in a fine matrix (Fig. 5c). The minerals have moderate to strong undulose extinction, are stretched in the mylonitic foliation and cataclased. In alvikite and calc-silicate mylonitic bands, calcite largely replaces actinolite, biotite and apatite. The carbonates analyzed with EDS contain Sr in their structure. The absence of Sr in some analyzed carbonate samples including veinlets suggests a mineral generation not related to the carbonatite system.

Apatite occurs as anhedral or subhedral crystals less than 0.8 mm in size, with moderate to strong undulose extinction, stretched along the protomylonitic foliation and showing some cracks filled with recrystallized calcite and monazite (Fig. 5d). Every apatite analyzed using the EDS was classified as fluorapatite with Sr. Multiple crystals of magnetite, ilmenite and ilmenorutile are common, typically anhedral, 5–10 mm in size (rarely > 1 cm). These crystals may be concentrated to form larger aggregates. In Passo Feio alvikite samples, ilmenite is common as lamellae in magnetite and as discrete platy crystals < 0.5 mm in length. All observed rutile forms very fine-grained aggregates, probably developed at the expense of ilmenite. Every ilmenorutile described are intergrowth with ilmenite.

The most important Nb mineral recognized belongs to the pyrochlore group, has different alteration stages and referred to as pyrochlore-like mineral. These minerals form disseminated fine to coarse-grained elongate to anhedral crystals ranging in color from yellow to dark red (Fig. 5e). The crystals occur as disseminations in the carbonate matrix along the foliation and can form aggregates with ferrocolumbite (Fig. 5f), or incomplete pseudomorphs of barite and bastnaesite (Fig. 6a). Pyrochlore-like minerals show compositional variation and discernible zoning in BSE, with variable contents of Nb, Ti, Th, U, Ca, Fe and REE. Other minerals with some Nb are found in Ti and Fe phases, which are oxide minerals. Among rock-forming minerals, ilmenite and rutile are the only significant Nb hosts, presenting the same petrographic characteristic of ilmenite and rutile devoid of Nb. Columbite was found in one alvikite sample. Carbonates and phosphates are essentially devoid of detectable Nb using EDS analyses.

Minerals containing REE are present in all carbonatite units and include monazite, pyrochlore-like minerals, bastnaesite, allanite and rontgenite. Monazite occurs as isolated crystals in carbonate matrix or included in minerals such as apatite, ilmenite, ilmenorutile and biotite, sometimes filling fractures in apatite and biotite. Less commonly, there is bastnaesite, allanite and rontgenite replacing pyrochlore-like minerals.

Baddeleyite occurs as crystals dispersed in the carbonate matrix, in places surrounded by a narrow zircon overgrowth (Fig. 6b), and also as inclusions in thorite and pyrochlore-like mineral aggregates (Fig. 6c). Euhedral trace zircon is common as

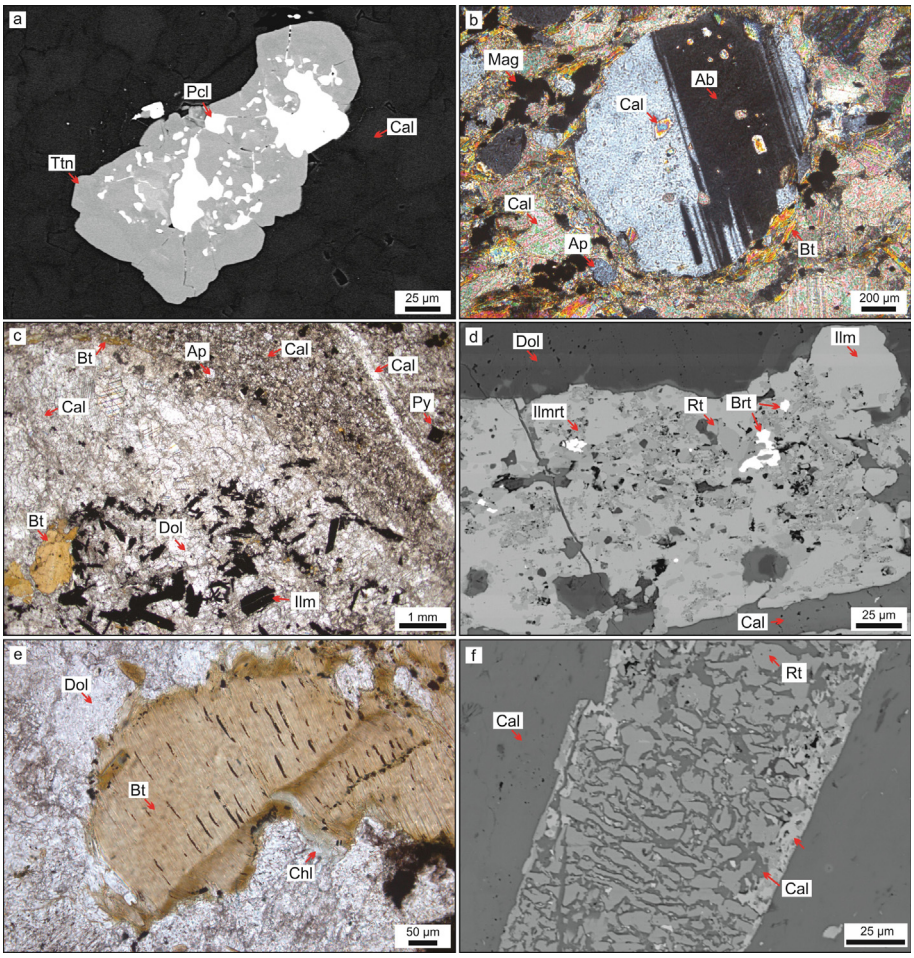

Fig. 7. Selected textural characteristics of Passo Feio and Picada dos Tocos carbonatites: (a) titanite with pyrochlore-like minerals inclusions in backscattered electron image (BSE); (b) rounded albite grain with thermal erosional boundary and substituted by calcite dispersed in a carbonate matrix in cross-polarized light (XPL); (c) textural relationship between beforsite xenolith and foliated alvikite, in plane-polarized light (PPL); (d) ilmenite, rutile and ilmenorutile intergrowth with barite inclusions in dolomitic matrix, and calcite veinlets; (e) biotite showing kink bands and alteration to chlorite (PPL); (f) graphic texture in a rutile/ilmenite grain close to xenolith border. Ab – albite, Ap – apatite, Brt – barite, Bt – biotite, Cal – calcite, Chl – chlorite, Dol – dolomite, Ilm – ilmenite, Ilmrt – ilmenorutile, Pcl – pyrochlore-like mineral, Py – pyrite, Rt – rutile, Ttn – titanite.

cumulate bipyramidal crystals in beforsite (typical of alkaline rocks, Corfu et al., 2003), zoned, up to 0.1 mm in size, associated with apatite and REE minerals (Fig. 6d). Zircon is dispersed in the alvikite, with crystals up to 30 μm in size.

Titanite occurs as prismatic zoned crystals, eventually rounded, with different Fe and Ti contents. Two types of titanite were found. The first has inclusions of ilmenite, ilmenorutile and pyrochlore-like minerals (Fig. 6e). The second one has a clean surface, growth along the biotite/chlorite cleavages (Fig. 6f) and can have pyrochlore-like minerals filling some fractures (Fig. 7a). Optically, both titanites are indistinguishable. It is likely that the titanite with inclusions is igneous, the other one metamorphic.

Biotite with less than 3.0 mm size is interstitial or isolated in the carbonate matrix with lamellae following protomylonitic orientation. The integrated use of texture, petrography and BSE features shows the similarity between biotite from the carbonatite and from the host rock. The only distinction is the presence of inclusions of pyrochlore-like minerals and apatite in the magmatic biotite.

Other accessory minerals, including pyrite and chalcopyrite, are common pervasive or filling fractures. Chlorite grew replacing mainly biotite and actinolite as ripiform crystals aligned in the foliation and associated with biotite in mylonitic bands. Chlorite also occurs filling fractures and eventually surrounding plagioclase grains in calc-silicate layers corroded by carbonates (Fig. 7b).

One xenolith of globular beforsite in an alvikite sample (Fig. 7c) has abundant dolomite, biotite, intergrowths of ilmenite, rutile and ilmenorutile (Fig. 7d). Pyrochlore-like minerals, monazite, barite and thorite are present as trace minerals. Kink bands and chloritization of biotite are observed (Fig. 7e). Close to the border, graphic relations in ilmenite/rutile crystals can be observed (Fig. 7f). This xenolith may suggest more than two intrusive carbonatite events.

Throughout the intrusion, alvikite hosts numerous, partially digested xenoliths of silicate rocks, most of which are fine-grained, foliated biotite amphibolite described below. Very fine-grained quartz-feldspar centimetric xenoliths were also observed in alvikite portions, in all cores (Fig. 4f). These rocks comprise sub-rounded quartz, feldspar and iron oxides, apparently banded (or foliated). The characteristics are similar to those observed in facies of Bom Jardim Group. They are also described in low-grade metamorphics from the Passo Feio Complex (Fragoso-Cesar, 1991). More studies are needed to define the stratigraphy of the xenoliths.

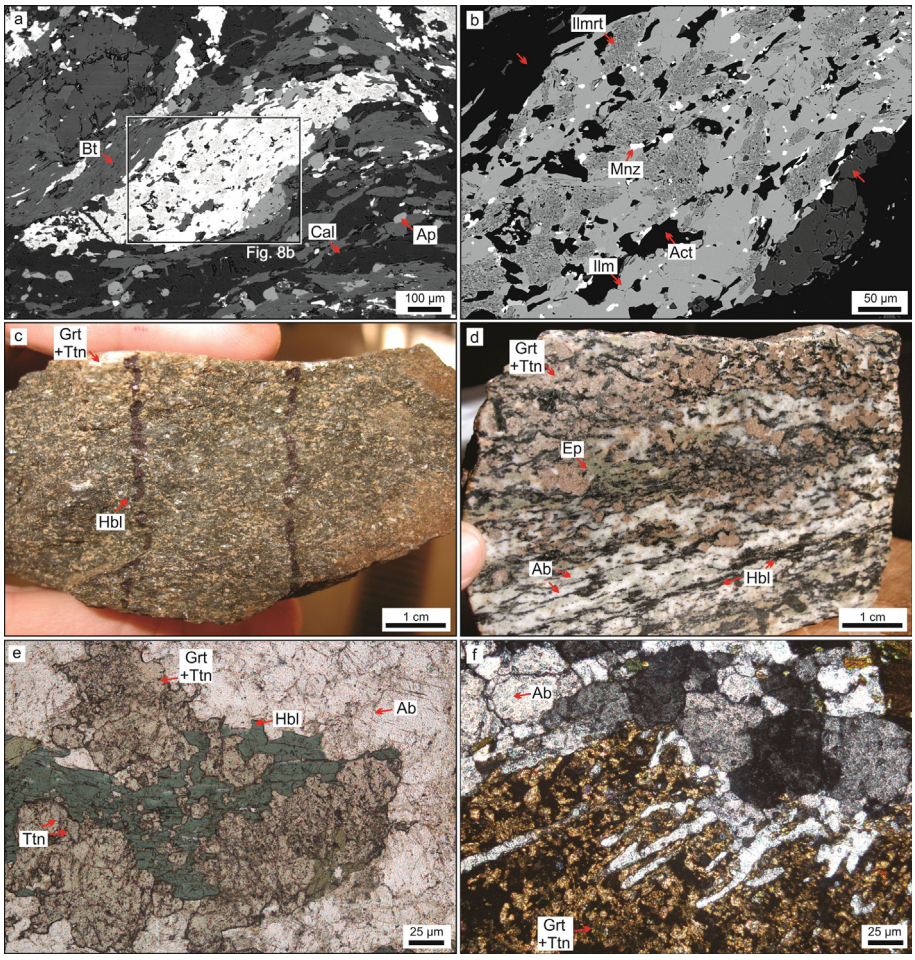

Fig. 8. Selected textural characteristics of Picada dos Tocos biotite amphibolite (a and b): (a) polycrystalline ilmenite/ilmenorutile aggregate, e.g. sigmoid in backscattered electron image (BSE); (b) detail of Fig. 8a showing overgrowth of ilmenite and ilmenorutile with monazite inclusions, and apatite growth mainly bordering ilmenite/ilmenorutile grains (BSE). Passo Feio titanite hornblende granofels (c to f): (c) titanite hornblende granofels sample showing nematoblastic hornblende replaced by garnet and titanite, in hand sample; (d) sample close to the carbonatite contact, showing needle-shaped hornblende replaced by garnet and titanite intergrowth, strong albitization and bands with epidotization, hand sample; (e) titanite and garnet replacing hornblende in plane-polarized light (PPL); (f) albite replacing titanite and garnet intergrowth in cross-polarized light (XPL). Ab – albite, Act – actinolite, Ap – apatite, Bt – biotite, Cal – calcite, Ep – epidote, Grt – garnet, Hbl – hornblende, Ilm – ilmenite, Ilmrt – ilmenorutile, Mnz – monazite, Ttn – titanite.

Table 1
Representative bulk-chemical analyses of Caçapava do Sul carbonatites. Major elements in wt% and trace elements in ppm. Rock abbreviations: beforsite (Mc), alvikite (Cc), biotite amphibolite (Ba) and titanite hornblende granofels (Thg).

Sample Borehole/depth (m)Rock type	TA2 2/234.7 Mc	TA3 2/235.1 Mc	TA9 4/45.0 Mc	TA19 5/52.35 Mc	TA20 5/54.25 Mc	TA1 2/199.8 Cc	TA5 2/237.2 Cc	TA8 2/239.4 Cc	TA9-10 4/45.05 Cc	TA11-12 4/45.3 Cc
SiO_2	0.71	2.01	0.79	1.88	6.71	4.45	1.44	9.26	0.83	0.77
TiO_2	0.03	0.02	0.07	0.10	0.18	0.68	0.02	2.34	0.02	0.01
Al_2O_3	0.13	0.15	0.23	0.27	0.61	1.26	0.15	3.16	0.26	0.18
FeO(t)*	2.40	3.33	2.64	2.55	3.32	4.02	2.30	6.07	2.70	0.53
MnO	0.43	0.42	0.43	0.51	0.32	0.20	0.54	0.43	0.20	0.16
MgO	17.50	14.50	17.15	9.59	10.70	2.38	5.50	5.80	2.40	1.90
CaO	33.0	34.7	31.8	41.50	36.90	47.9	46.9	38.7	50.3	52.4
Na_2O	0.02	0.03	0.03	0.02	0.02	0.05	0.02	0.07	0.02	0.03
K_2O	-	-	-	0.01	0.07	0.06	-	1.27	0.04	0.05
SrO	0.42	0.38	0.42	0.37	0.36	0.57	0.22	0.42	0.62	0.70
BaO	-	-	0.03	0.01	0.23	0.01	-	0.08	0.03	0.05
P_2O_5	2.68	5.58	2.00	4.71	8.38	2.72	5.31	3.17	4.46	1.67
LOI	41.5	36.8	42.9	37.8	29.9	35.3	36.6	28.6	37.3	41.4
Total	98.83	98.18	98.49	99.33	97.70	99.61	99.00	99.37	99.18	99.85
V	27	72	18	43	70	121	72	249	46	14
Cr	10	10	10	20	20	30	10	10	20	10
Co	21	7	12	8	11	14	6	26	4	3
Ni	7	8	7	14	17	12	8	25	8	7
Cu	5	1	8	8	11	34	2	70	4	2
Zn	34	24	37	37	30	34	10	113	9	10
Rb	0.2	0.2	0.5	0.2	1.6	1.5	0.2	29	1.0	1.0
Y	42.8	45.7	33.4	190.0	82.4	56.9	52.2	94.8	85.8	85.9
Zr	30	106	26	1460	140	134	117	253	221	111
Nb	1010	>2500	448	859	1530	543	>2500	1015	162	158
La (ppm)	127	209	120	552	259	265	190	331	261	258
Ce	342	543	287	1095	646	542	531	606	581	523
Pr	44.7	68.6	37.4	140.0	84.7	62.5	70.2	72.3	69.4	67.8
Nd	171	269	146	536	339	226	279	267	277	261
Sm	27.3	42.5	24.9	94.3	58.6	33.7	46.0	45.8	49.3	44.0
Eu	7.31	10.85	6.62	24.30	14.75	9.34	11.00	12.65	13.60	12.15
Gd	17.8	26.6	15.9	60.5	36.0	22.2	26.1	29.7	36.6	31.1
Tb	2.19	3.15	2.01	7.65	4.30	2.71	3.15	3.90	4.66	4.02
Dy	10.65	14.30	9.02	39.30	21.70	13.40	14.65	20.80	22.00	20.30
Ho	1.60	1.98	1.33	6.67	3.24	2.14	2.06	3.30	3.66	3.23
Er	3.90	4.27	2.84	18.95	7.55	5.03	4.42	8.35	8.20	7.68
Tm	0.43	0.47	0.32	2.80	0.91	0.63	0.47	1.08	0.99	1.00
Yb	2.29	1.98	1.80	18.02	5.20	3.45	2.56	6.79	5.33	5.62
Lu	0.28	0.28	0.22	2.80	0.68	0.44	0.30	0.94	0.73	0.73
Hf	0.4	1.1	0.4	16.2	2.0	2.8	1.1	6.3	1.7	1.1
Th	40.8	59.1	71.7	173.5	327.0	24.5	84.3	190.0	152.5	130.5
U	5.1	2.5	12.1	8.0	56.2	28.0	2.6	59.8	23.3	23.1
ΣREE	758.9	1196.0	655.9	2598.5	1481.6	1188.5	1181.4	1409.6	1333.5	1239.6
$La/Lu_{(n)}$	47.08	77.48	56.85	20.46	39.53	62.51	65.91	36.55	37.11	36.68

Sample Borehole/depth (m) Rock type	TA16 4/51.5 Cc	TA18 5/21.0 Cc	TA25 5/64.41 Cc	TA26 5/67.25 Cc	TA23 5/54.4 Cc	PF Outcrop Cc	TA10 4/45.1 Ba	TA21 5/54.3 Ba	TA24 5/64.37 Ba	TA1320 Outcrop Thg	PF1 Outcrop Thg
SiO_2	7.23	1.15	2.25	11.30	2.43	5.48	30.40	35.90	20.20	46.50	36.30
TiO_2	0.66	0.03	0.10	1.69	0.04	0.48	4.09	3.66	3.09	1.45	5.34
Al_2O_3	2.02	0.17	0.56	3.66	0.94	0.41	9.61	10.50	4.16	16.50	9.89
FeO(t)*	4.62	3.77	3.08	6.22	7.17	9.25	12.05	12.95	10.05	9.84	17.15
MnO	0.18	0.25	0.24	0.30	0.20	0.35	0.22	0.15	0.35	0.17	0.32
MgO	2.98	3.43	3.94	6.92	3.13	3.60	8.82	9.83	14.85	2.23	5.98
CaO	45.3	48.60	46.60	37.20	45.80	44.70	14.4	11.45	19.80	13.00	18.75
Na_2O	0.55	0.04	0.14	0.10	0.09	0.17	2.25	1.58	0.44	5.01	1.79
K_2O	0.64	0.02	0.15	0.89	0.05	0.02	3.53	2.29	2.44	0.68	0.91
SrO	0.62	0.71	0.64	0.22	0.46	0.52	0.16	0.13	0.21	0.43	0.06
BaO	0.08	0.05	0.07	0.09	0.02	0.02	0.12	0.17	0.12	0.04	0.02
P_2O_5	3.55	3.12	5.65	5.68	9.55	2.88	2.02	0.84	3.22	1.25	1.12
LOI	32.0	37.8	34.4	24.8	28.5	32.3	10.55	10.45	19.55	1.22	1.18
Total	100.43	99.14	97.82	99.07	98.38	100.10	98.23	99.95	98.49	98.30	98.82
V	140	76	60	192	72	227	398	373	257	358	640
Cr	10	30	10	20	10	10	100	370	10	10	60
Co	11	16	17	26	7	12	48	54	30	18	49
Ni	11	5	8	27	10	13	54	200	28	2	46
Cu	14	16	17	26	7	12	35	54	30	18	49
Zn	61	36	35	64	25	185	96	106	176	50	134
Rb	19.5	0.5	3.8	20.7	1.2	0.3	99.0	64.2	64.3	7.2	4.4
Y	78.5	91.6	106.0	86.6	91.0	58.5	47.2	36.5	63.6	34.0	80.2
Zr	220	32	120	354	761	98	384	322	281	392	578
Nb	127	826	1845	1530	85	166	384	184	1140	46	239

(*continued on next page*)

Table 1 (*continued*)

Sample Borehole/depth (m) Rock type	TA16 4/51.5 Cc	TA18 5/21.0 Cc	TA25 5/64.41 Cc	TA26 5/67.25 Cc	TA23 5/54.4 Cc	PF Outcrop Cc	TA10 4/45.1 Ba	TA21 5/54.3 Ba	TA24 5/64.37 Ba	TA1320 Outcrop Thg	PF1 Outcrop Thg
La (ppm)	335	269	322	222	300	229	142	84	284	40	90
Ce	662	580	711	572	652	483	292	173	590	71.3	271
Pr	83.9	74.9	93.0	77.1	88.1	53.7	36.3	22.4	72.1	8.23	30.6
Nd	306	291	366	307	347	207	137	87	269	35	128
Sm	47.2	49.1	62.7	54.9	60.6	33.0	25.3	16.4	45.3	7.7	23.8
Eu	12.85	13.80	18.05	15.80	15.65	9.18	6.93	4.50	12.05	2.57	6.95
Gd	31.0	34.3	43.0	37.3	40.1	23.6	17.7	11.5	28.2	7.6	20.3
Tb	3.94	4.43	5.35	4.80	4.69	2.93	2.29	1.57	3.68	0.93	2.96
Dy	18.15	22.30	27.30	23.70	22.80	13.55	11.75	7.73	17.85	5.00	15.60
Ho	2.91	3.67	4.22	3.52	3.53	2.22	1.85	2.28	2.57	0.93	2.96
Er	6.78	8.94	9.70	8.01	7.87	5.08	4.25	3.02	5.68	2.72	7.51
Tm	0.80	1.15	1.21	0.91	0.96	0.62	0.52	0.40	0.75	0.41	0.96
Yb	4.13	6.02	6.94	5.08	4.76	3.53	2.60	2.32	3.80	2.59	5.89
Lu	0.53	0.80	0.91	0.61	0.68	0.42	0.33	0.31	0.44	0.37	0.82
Hf	3.7	0.6	1.8	6.0	8.2	1.7	8.7	7.5	6.8	5.9	12.8
Th	17.5	156.5	354.0	185.0	933.0	9.87	50.8	29.2	256.0	3.68	27.6
U	4.6	9.9	72.5	26.1	50.7	6.4	12.5	10.1	95.3	6.1	5.8
ΣREE	1515.2	1359.4	1671.4	1332.7	1548.7	1066.8	681.3	415.1	1335.7	185.6	608.4
$La/Lu_{(n)}$	65.61	34.90	36.73	37.78	45.79	56.59	44.66	28.13	67.00	11.22	11.46

FeO(t) = Total Iron; ΣREE = Total Rare Earth Elements. (–) Below detection limit (K_2O, BaO).

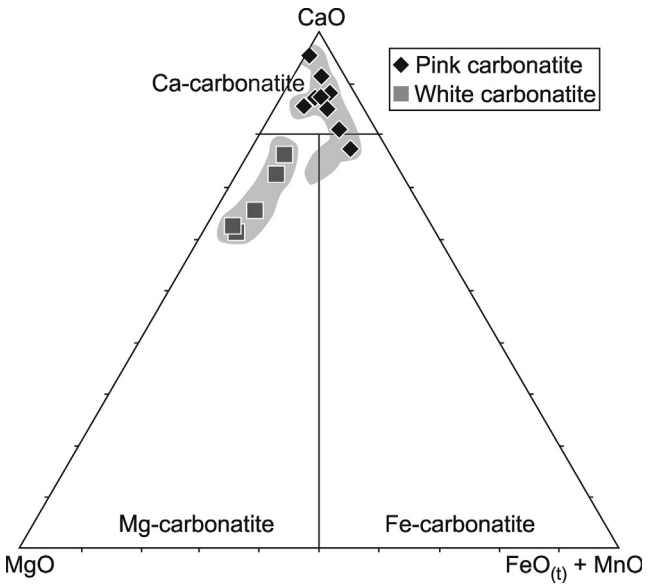

Fig. 9. Carbonatite ternary CaO – MgO – ($FeO_{(t)}$ + MnO) discrimination diagram after Woolley and Kempe (1989) for Caçapava do Sul samples. The carbonatite plots between the fields of calciocarbonatite and magnesiocarbonatite. $FeO_{(t)}$ = total iron.

5.1.2. Biotite amphibolites

Biotite amphibolites enveloping carbonatites in the Picada dos Tocos occurrence exhibit a penetrative foliation and are composed of calcite, biotite, actinolite, hornblende, chlorite, apatite, magnetite, ilmenite, ilmenorutile, pyrite, chalcopyrite and minor plagioclase, pyrochlore, quartz, monazite, pyrite, zircon and titanite; locally, clinopyroxene (augite and diopside-hedenbergite) relics are present. The mylonitic texture is evidenced mainly by strong stretching and alignment of calcite, biotite, amphiboles, chlorite, apatite and magnetite. The essentially ductile shearing also caused boudinage of actinolite and apatite, which have synthetic fractures and pressure shadows with calcite. Subsequently, brittle tectonics caused fragmentation and brecciation of the rock, with cracks and fissures filled by biotite, calcite and chlorite, suggesting hydraulic fracturing.

Calcite granoblastic aggregates in aligned bands along the axial plane of micro and mesofolds developed in biotite aggregates. They replaced intensely biotite and actinolite, as well as apatite with the CO_2 infiltration under a predominantly ductile shear regime.

Biotite is lamellar and strongly oriented, showing tight bends slightly open with transposition flanks, kink bands and recrystallizing in the axial plane, with strong undulose extinction. The mineral was intensely replaced by chlorite, calcite, apatite, titanite and opaque minerals. Chlorite can be lamellar and fibrous, grown from biotite by replacement due to hydrothermalism, and also filling cracks.

The amphiboles (actinolite, hornblende) are ripiform, oriented in the mylonitic foliation, boudinaged and consumed by calcite and apatite. The plagioclase, with polysynthetic twinning and intense undulose extinction, occurs preferably in the biotitic layers, aligned to the foliation.

Opaque minerals are magnetite, ilmenite, ilmenorutile and pyrite. Some of the pyrite is idiomorphic. They all show growth relationships from biotite, and mobilized forming aggregates along the fissures, associated with chlorite. Ilmenite and ilmenorutile aggregates exhibit patchy or speckled zoning due to extreme variations in Fe, Ti and Nb content (Fig. 8a and b). Titanite is idiomorphic, grew in biotite and actinolite, and occurs locally.

Close to the contact with sediments of the Bom Jardim Group, the rock displays cataclastic features with cracks filled by chlorite, opaque minerals, calcite and rarely quartz. Although there is a predominance of fragments relative to matrix, intense local cataclase generated ultracataclasite.

The conditions for dynamic metamorphism are lower greenschist facies involving chlorite associated with calcite and opaque minerals under an essentially brittle system affecting the protolith. Later, with the carbonatite intrusion, this package was affected by cataclase accompanied by CO_2 and H_2O infiltration, causing intense chloritization of amphibole and pyroxene and carbonation/saussuritization of plagioclase.

5.1.3. Titanite-hornblende granofels

The titanite-hornblende granofels from the Passo Feio occurrence are essentially medium-grained with granoblastic texture (Fig. 8c). They are composed of hornblende and titanite, with accessory phases observed including apatite, biotite, pargasite, ilmenite, actinolite, zircon and epidote. Hornblende aggregates are locally aligned, and interpreted as a sub-solidus tectonic struc-

ture. Close to the contact with carbonatites, coarse grained garnet and abundant albite are common (Fig. 8d).

The hornblende is anhedral to subhedral, needle-shaped, commonly showing scalloped to embayed grain boundaries; in some grains, titanite aggregates exhibit moderate to strong undulose extinction. The aligned aggregates suggest tectonic deformation, replaced by titanite, garnet and epidote (Fig. 8e) under conditions of amphibolite and lower/upper greenschist facies.

The titanite occurs usually as a millimetric to centimetric aggregates, interstitial and also coalescencing crystals replacing hornblende grains. The titanite frequently shows inclusions and intergrowths with garnet. The garnet was identified using EDS as grossular, and occurs in rocks close to the carbonatite contact, with grain size > 1.0 mm. Textural observations show garnet growing by coalescence in atoll texture, surrounding hornblende and intergrown with titanite.

Albite with polysynthetic twinning and intense undulose extinction is abundant close to the carbonatite contact, strongly replacing the garnet/titanite intergrowth (Fig. 8f). Apatite is anhedral, in a few cases subhedral, interstitial or forming aggregates. Biotite and pargasite are interstitial, fine-grained, with heterogeneous distribution, but biotite also occurs as inclusions in hornblende. Zircon is subhedral, fine-grained, included in titanite. Rare anhedral celestine grains occur isolated in the hornblende matrix. Epidote forms granoblastic aggregates elongated parallel to the foliation, resulting from partial hornblende replacement. Iron oxide occurs mainly filling fractures.

5.2. Whole-rock geochemistry

Twenty-one bulk rock chemical analyses for major and trace elements of carbonatites, biotite amphibolites and titanite hornblendite are sown in Table 1. Carbonatite data are plotted on the Woolley and Kempe (1989) classificatory diagram, shown in Fig. 9. Overall, the Ca-carbonatites lie above the 80% CaO reference line, and the Mg-carbonatites lie between 60% and 80% CaO, all less than 20% $FeO_{(t)}$. One sample plots in the Fe-carbonatite field because of the high magnetite and biotite contents, with no Fe carbonates present. Two samples plot between Mg- and Fe-carbonatites because they are a mechanical mixture of alvikite, beforsite and biotite amphibolite.

Variations in the modal proportions of biotite, amphibole and apatite cause variation of SiO_2, Al_2O_3, Na_2O, K_2O and P_2O_5. Chemistry of alvikite and beforsite is similar and displays the same ranges of trace element abundances and distribution with typical LREE enrichment (Table 1, Figs. 10–12).

Carbonatites and mafic rocks are distinguished on the basis of elemental distribution. The carbonatites have high levels of CaO, P_2O_5, Nb and Sr. Mafic host rocks, on the other hand, contain relatively high contents of SiO_2, Al_2O_3 and $FeO_{(t)}$; notably they also have significant values of TiO_2, Rb, Nb and Sr, but erratic CaO, Na_2O, K_2O and MgO.

The relatively higher values of SiO_2 and $FeO_{(t)}$ observed in alvikite when compared to beforsite suggest that alvikite silicate and iron-rich minerals crystallized during the early stages of carbonatite magmatic evolution. However, host rock assimilation could

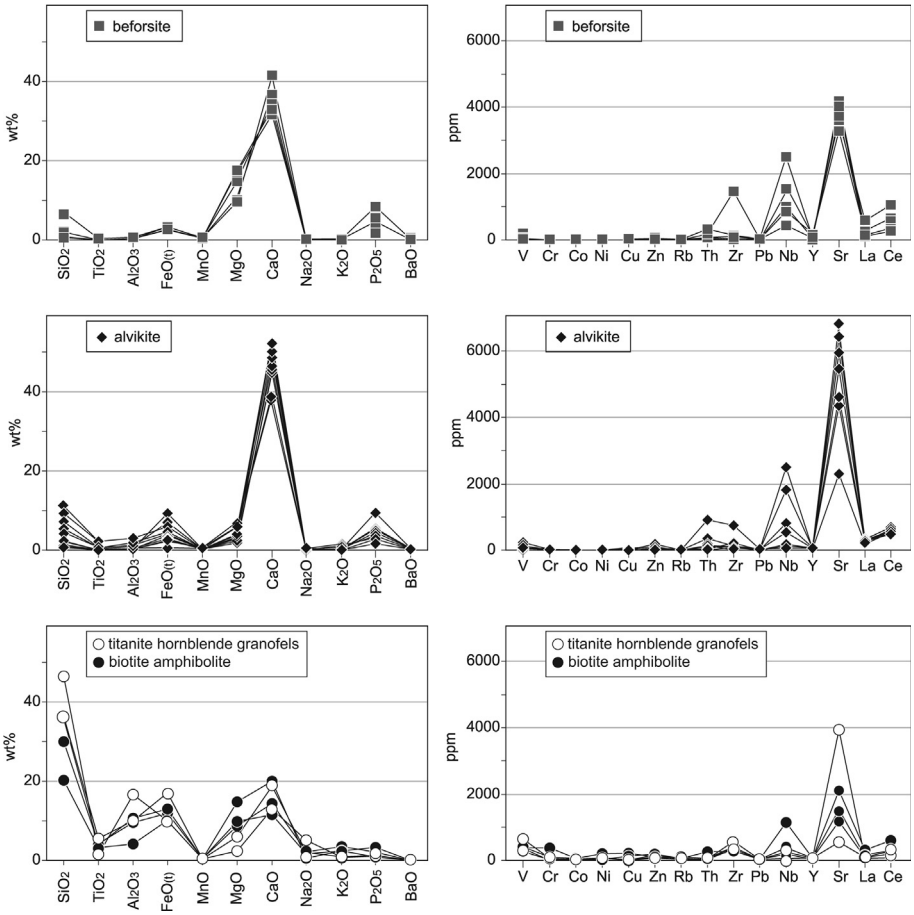

Fig. 10. Average composition of beforsite, alvikite, biotite amphibolite and titanite hornblende granofels.

contribute significantly with these components. Alkali concentrations are very low in all the carbonatites samples. Although carbonatite melts are rich in K and Na (Woodard and Hölttä, 2005), some studies report K- and Na-poor carbonatite magmas as Barker and Nixon (1989) at Fort Portal, Uganda, and Ignacio et al. (2012) at São Vicente, Cape Verde Islands. The Caçapava do Sul carbonatites lack alkalis, but the enrichment in one Passo Feio fenite sample suggests that the carbonatite magma contained some Na but was relatively poor in K.

Some relevant plots are shown in Fig. 11 to evaluate the characteristics and evolution of both carbonatites. A negative correlation between CaO and SiO_2 is observed in alvikite samples, and similar behavior is seen between MgO and SiO_2 in beforsite samples, probably due to variations in Ca and Mg activities with the fractionation of silica minerals during carbonatite evolution. A positive correlation between TiO_2-SiO_2, Al_2O_3-SiO_2 and $FeO_{(t)}$-SiO_2 mainly in alvikites could also be explained by the abundant Ti-rich biotite in the host rocks and xenolith content. A positive correlation can be observed between SiO_2 and P_2O_5 in beforsites and alvikites with low silica, suggesting a depletion of these elements with the carbonatite magmas evolution. A positive correlation between CaO and P_2O_5 with ΣREE (Total Rare Earth Elements) and a negative correlation between MgO and ΣREE is restricted to beforsite samples, while the positive correlation between Ba and ΣREE is an exclusive alvikite characteristic. A negative correlation between CaO and MgO, which can be referred to as mineral ratio (e.g. calcite/dolomite in carbonatites), characterizes all studied carbonatites. Sr is variably enriched and shows erratic variation (0,37–0,42 SrO% in beforsites and 0,22–0,71 SrO% in alvikites). In alvikites, Sr has negative correlation with MgO and positive correlation with CaO, but opposite behavior is observed in beforsites.

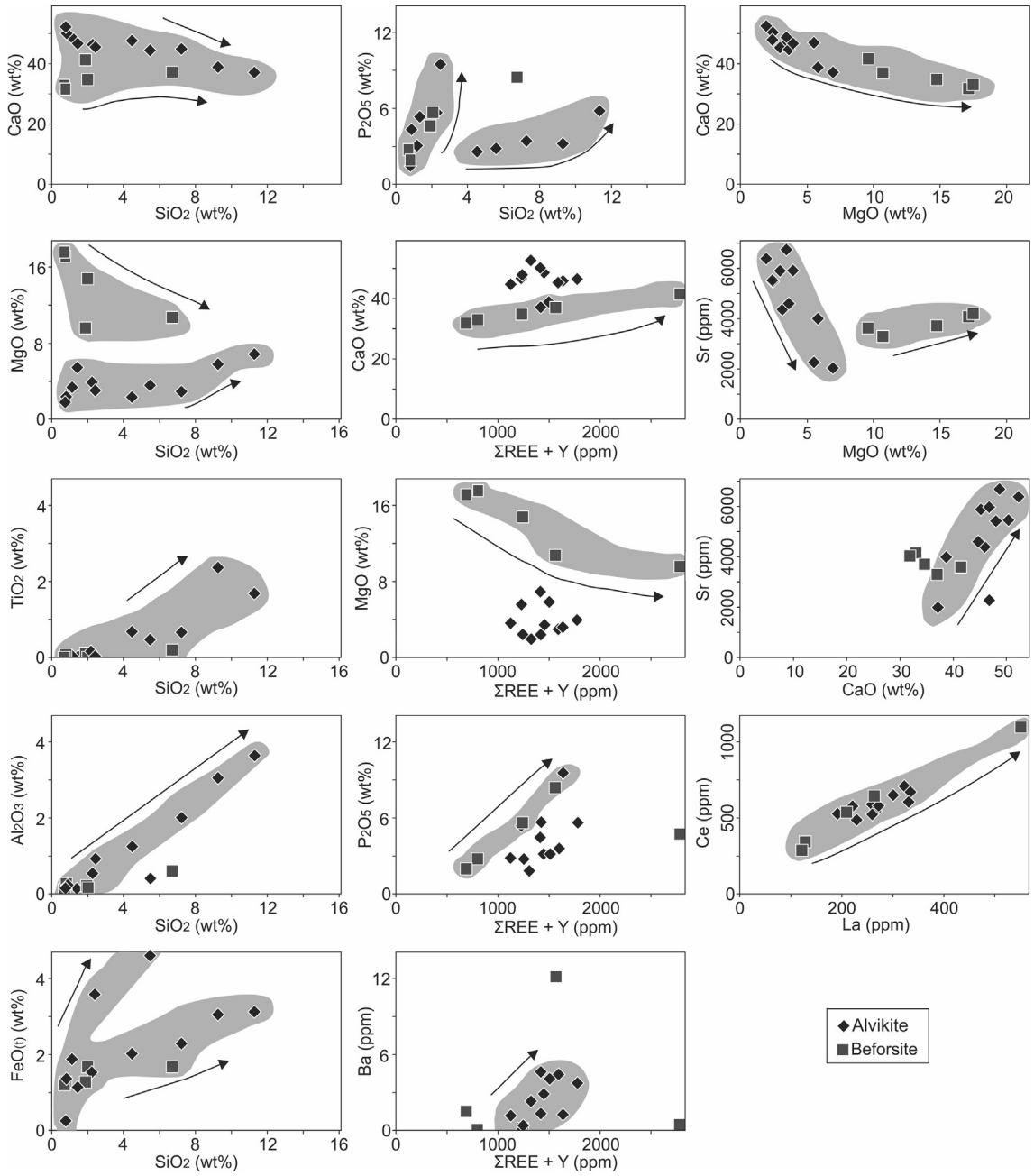

Fig. 11. Correlation of selected major element oxides and trace elements of Caçapava do Sul carbonatite samples.

The analyzed samples have relatively lower Nb contents compared to carbonatites from the literature (cf. Woolley and Kempe, 1989): 85.4 to >2500 ppm for alvikites and 448 to >2500 ppm for beforsites. For alvikite and beforsite, ΣREE vary within the intervals 1067–1671 ppm and 275–2599 ppm, respectively (Table 1). Fig. 11 shows the variation of the La and Ce contents along the evolution of these rocks. The REE abundances were normalized to chondrite using the primitive mantle values of McDonough and Sun (1995), that represent CI (carbonaceous) chondrites, which contain carbon, water and other volatile elements. The values (Fig. 12) show a large enrichment when compared with other terrestrial rocks and a strong fractionation between light and heavy REE (LREE and HREE). All samples are LREE-enriched with $La_{(n)}/Lu_{(n)}$ ratios of 20.46–77.48 for beforsites and 34.90–65.91 for alvikites ($La_{(n)}/Yb_{(n)}$beforsite = 20.60–71.71 and $La_{(n)}/Yb_{(n)}$alvikite = 29.69–55.10).

At the current stage of study, the magma evolution for the carbonatite is tentatively suggested as an early alvikite to a late beforsite.

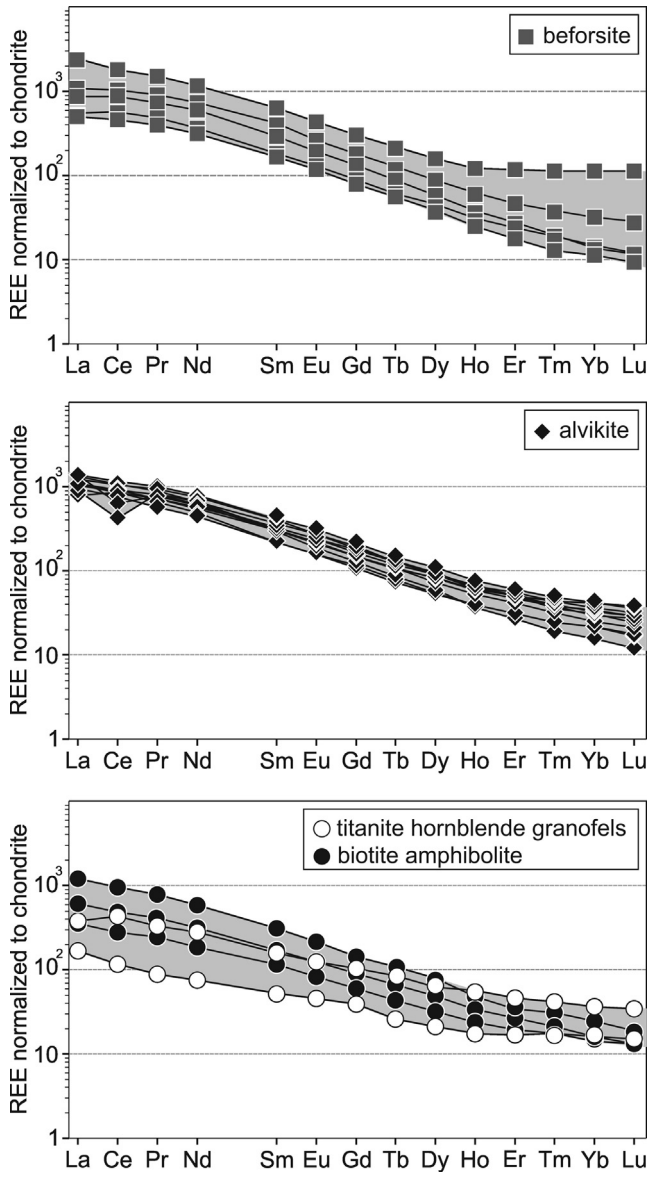

Fig. 12. Chondrite normalized REE diagram (McDonough and Sun, 1995) for the studied carbonatites and mafic rocks.

5.3. Geochronology

Based on field relationships, the relative age of the carbonatite system is interpreted as older than the Caçapava do Sul granite intrusion. The LA-ICP-MS dating of zircon grains from one representative sample of beforsite yields significant information regarding the age of the rock, corroborating the field observation, and established an absolute timeframe for the emplacement of the studied carbonatite. The analyzed zircons have short prismatic and bipyramidal habits and show a diameter between 40 and 100 μm, aspect ratio close to 1. Internal structures observed in CL and BSE show concentric planar zonation indicating igneous origin for zircons (Corfu et al., 2003). The Th/U ratios (2.1–5.43) are high and typical of mantle-derived zircon (e.g.; Hoskin and Ireland, 2000; Pinto et al., 2011), reflecting the unusual low U and moderate to relatively high Th concentrations in zircons from carbonatites (Belousova et al., 2002).

Eight zircon grains were analyzed, and four have anomalously high content of common-Pb resulting in a large uncertainty, so these samples were rejected for calculation of the age. However, four zircon spots have concordant U-Pb data and yield an age of 603 ± 4.5 Ma interpreted as the igneous crystallization age of the Picada dos Tocos beforsite, as shown in Table 2, Figs. 13 and 14.

This Caçapava do Sul carbonatite age is within the 650–500 Ma (Late Neoproterozoic-Cambrian) worldwide alkaline post-collisional magmatism described by Veevers (2004, 2007), that includes A-type granite, nepheline syenite and carbonatite associated with arcs that include rift and extensional environment, denoting crustal extension. Furthermore, during the Ediacaran, a collision of the Rio de La Plata and Encantadas microcontinent was described followed by a transpressive tectonism and volcanic activity with shoshonitic, high-K calc-alkaline and tholeiitic characteristics (Saalmann et al., 2010; Philipp et al., 2016 and references therein). Probably the carbonatite intrusion is related to one of these events.

6. Tectonic setting

Primary carbonatite magma can be generated from mantle peridotite, with magnesian composition, and the reaction of the lherzolite to wehrlite mantle leading to the production of calciocarbonatite magmas (Wyllie, 1989; Wyllie and Lee, 1998; Dalton and Wood, 1993; Woodard and Hetherington, 2014). Other studies suggest carbonatites to be derived from the melting of recycled carbonated oceanic crust (eclogite) (Hoernle et al., 2002; Doucelance et al., 2010; Hammouda and Keshav, 2015). Experiments of Hammouda (2003) and Kiseeva et al. (2012) suggest that naturally calcic carbonatites could be the result of direct melting of carbonated eclogite. However, experimental results of Dasgupta et al. (2004) and Yaxley and Brey (2004) obtained magnesian liquids, showing it strongly relies on the starting composition. Because of the low volume and high reactivity of carbonatite magmas, as well as physico-chemical barriers, an extensional tectonic environment is needed to allow for rapid emplacement in the upper crust. Experiments done by Thomsen and Schmidt (2008) using complex systems, representing subducted carbonated pelitic sediments, resulted in potassic silicate and carbonatite melts immiscible under upper mantle conditions. Thus, partial melting of a subduction-enriched mantle could produce ultrapotassic or shoshonitic silicate melts with associated immiscible carbonatite (Woodard and Hetherington, 2014). Examples of carbonatites from post-collisional tectonic settings include Naantali, SW Finland (Woodard and Hetherington, 2014 and references therein), Hongcheon area, South Korea (Kim et al., 2016), Maoniuping, Lizhuang and Dalucao, Sichuan, China (Hou et al., 2006) and Eden Lake, Manitoba, Canada (Chakmouradian et al., 2008).

Table 2
Laser ablation ICP-MS U-Pb analyses of selected zircon. Conc. = Concórdia; Sam. = zircon samples.

Sam.	Isotopic ratios (± 1σ errors)			Age (± 2σ errors), Ga			Pb total%	Pb rad ppm	Th ppm	U ppm	Th/U	Conc. 206/238	Conc. 206/238
	$^{206}Pb/^{238}U$	$^{207}Pb/^{235}U$	$^{207}Pb/^{206}Pb$	$^{206}Pb/^{238}U$	$^{207}Pb/^{235}U$	$^{207}Pb/^{206}Pb$						207/235	207/206
2.1	0.0975 (0.0014)	0.7556 (0.0422)	0.0562 (0.0035)	0.600 (0.008)	0.571 (0.025)	0.460 (0.145)	7.42	19	235	91	2.58	104	130
3.1	0.0964 (0.0023)	0.7537 (0.0763)	0.0567 (0.0066)	0.593 (0.013)	0.570 (0.044)	0.480 (0.150)	2.00	20	327	73	4.49	104	123
5.1	0.0972 (0.0013)	0.7558 (0.0376)	0.0564 (0.0031)	0.598 (0.008)	0.572 (0.021)	0.468 (0.119)	1.79	22	240	102	2.36	104	127
8.1	0.1012 (0.0016)	0.8114 (0.0496)	0.0582 (0.0039)	0.621 (0.009)	0.063 (0.028)	0.536 (0.141)	2.96	26	512	94	5.43	103	116
	Zircons not used for age calculation												
1.1	0.0966 (0.0013)	0.7193 (0.0387)	0.0540 (0.0031)	0.595 (0.008)	0.550 (0.023)	0.371 (0.132)	20.84	16	193	92	2.10	108	160
4.1	0.0898 (0.0015)	0.7239 (0.0454)	0.0584 (0.0042)	0.555 (0.009)	0.553 (0.027)	0.546 (0.160)	6.51	16	233	70	3.33	100	101
6.1	0.1108 (0.0024)	0.8304 (0.0789)	00544 (0.0059)	0.677 (0.014)	0.614 (0.043)	0.387 (0.207)	6.62	15	231	49	4.75	110	175
7.1	0.0993 (0.0017)	0.7762 (0.0560)	0.0567 (0.0043)	0.610 (0.010)	0.583 (0.031)	0.479 (0.161)	9.52	19	277	83	3.36	104	127

Previous studies (e.g. Lima and Nardi, 1998; Paim et al., 2000; Sommer et al., 2006) show a shoshonitic to high-K calc-alkaline magmatic activity in Sul-Riograndense shield. Shoshonitic granitoids include the Lavras do Sul and volcanic equivalent Hilário andesites with associated lamprophyres. These rocks are related to the same event of carbonatite emplacement. Sommer et al. (2005) interpreted the magmatism from the melting of subducted rocks, whereas the high-Nb magmas display less influence of subduction-related metasomatism, and are closer to magmas produced from intraplate sources. Isotopic and geochronological data presented by Hartmann et al. (2011) indicate subduction processes between 900 and 700 Ma, resulting in the closure of an ocean and consumption of the oceanic liphosphere. Lima and Nardi (1998), however, considered that the differentiation processes of the shoshonitic magmatism had negligible crustal involvement.

The age results obtained in this study fit with the Dom Feliciano Belt tectonic model, where emplacement in the upper crust was facilitated by the reactivation of pre-existing deep shear zones and associated structures (e.g. Caçapava shear zone) at the onset of tectonic extension. The Caçapava do Sul carbonatites intruded parallel to a normal fault, close to a shear zone, which likely acted as a conduit for the carbonatite magma. Specific studies are needed to show the genetic relationship between shoshonitic and carbonatitic magmatism in the Sul-Riograndense Shield.

7. Discussion

In the Caçapava do Sul region, calcite, dolomite, apatite, REE and Nb minerals, barite, strontianite and thorite are associated with different phases of carbonatite intrusion and consequent hydrothermal alteration. According to Mitchel (2005a), in a sequence of carbonatites, a partial melting progress is marked by an increase in the activity of silica in the melt. As SiO_2 essentially participates in silicates, it decreased with the evolution of the carbonatite magma and silicates mostly crystallizing during the early stages (Gomide et al., 2016). Applying this reasoning, added to the

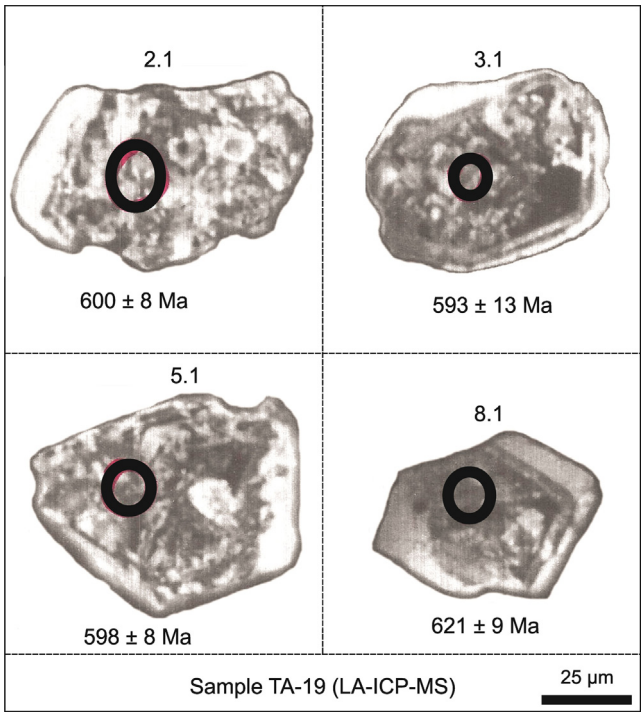

Fig. 13. Zircon cathodoluminescence (CL) images for the studied samples. The circles show LA-ICP-MS dating spots and corresponding U-Pb ages (in Ma).

petrographic observations, we can interpret that the Caçapava do Sul alvikite is more silicate enriched compared to beforsite and represents an early stage of the carbonatite magmatism. Nonetheless, the beforsite contains less Ba concentration than expected. The absence of sodic pyroxene, and rare fenitization processes may be related to the small dimension of bodies and primary magma chemistry.

Baddeleyite crystals enveloped by zircon, and thorite replacing pyrochlore-like minerals, indicate an increase in silica and thorium activity in the late evolution of the rock. The silica may be assimilated from metasedimentary silicate host rocks or can have a late hydrothermal origin. Petrography suggests that some biotite, titanite and amphibole are relics of the host rock, but titanite and biotite can also have an igneous origin related to carbonatite.

Low density and low viscosity characteristics of carbonatite magmas make cumulate processes and gravitational settling important aspects for their development (Kjarsgaard and Hamilton, 1989; Le Bas, 1989; Costanzo et al., 2006; Woodard and Hetherington, 2014). The presence of millimetric apatite banding supports our interpretation that the main foliation in the Caçapava do Sul carbonatites is primarily a magmatic feature linked to a synkinematic emplacement.

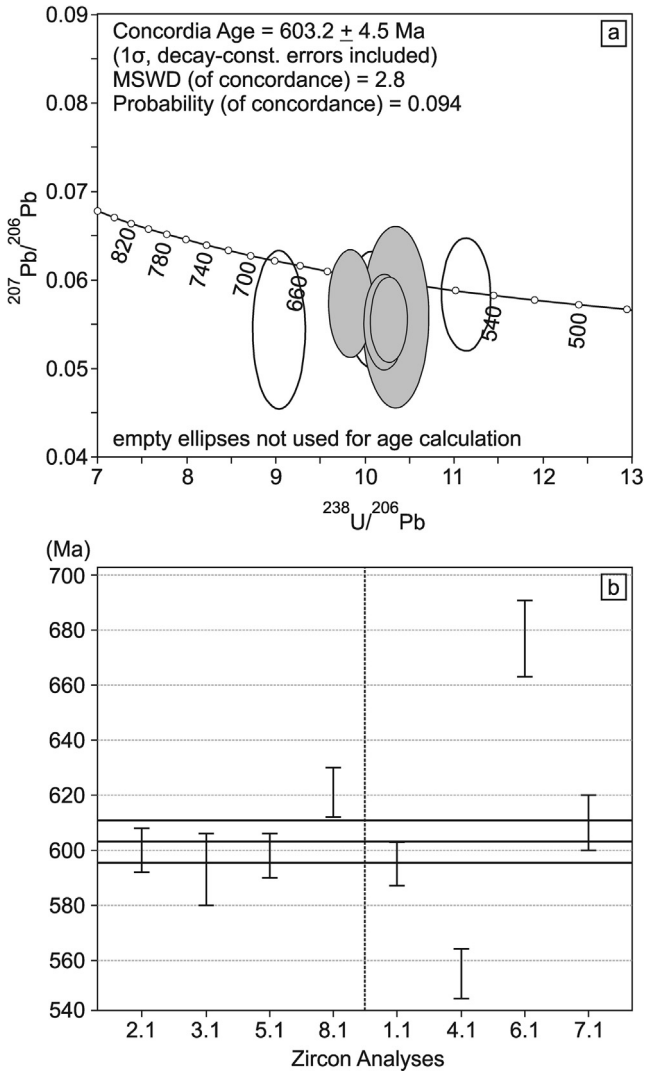

Fig. 14. (a) Isotopic analyses of zircon crystals displayed in a Tera-Wasserburg Concordia diagram; (b) error bar graph of the weighted average of $^{206}Pb/^{238}U$ ages. Error in 1σ.

Post-magmatic tectonic events and late hydrothermal phases are evidenced by small-scale folding of banding with minerals oriented with respect to the external regional foliation (host rocks), brecciation and presence of (1) chlorite pervasive calcite fracture filling, (2) associated veins filled by quartz and chlorite, (3) pyrite and less commonly chalcopyrite pervasive fracture filling, and (4) hematite fracture filling and crystallization along the foliation. Furthermore, the brecciation is localized, observed close to faults, suggesting that the Caçapava do Sul carbonatite was not an explosive event.

During the low-temperature hydrothermal processes that produced carbonate-chlorite-quartz veins, hydrothermal carbonate replaced the original magmatic carbonate in the carbonatite. These processes were unable to accommodate large cations such as Sr, and secondary carbonates formed without Sr. As a result, these elements preferentially partitioned into the hydrothermal fluid, which explains the occurrence of some free strontium carbonates in the matrix and veins. Following the indication of Mitchel (2005b), the significant presence of Nb, Ti and P, and low ΣREE, Sr and Ba concentrations suggests that the carbonatite is associated with the melilitite clan, although no associated silicate rocks were found.

There are no indications suggesting a parental relationship between the host mafic rocks and intruded carbonatites. The signature observed in aerogeophysics, especially in the Passo Feio occurrence, suggests that there is a much larger carbonatite system at depth than observed in outcrops. These bodies are probably interspersed with host rocks.

8. Conclusions

(1) The field relationships, mineralogy and geochemistry were used to study and characterize carbonatite dikes and sills in Caçapava do Sul, southernmost Brazil, as a first occurrence of carbonatite in the region.

(2) The discovery of carbonatite bodies in the Caçapava do Sul region, southern Brazilian Shield, led to the characterization of early alvikite, rich in host rock xenoliths, followed by late beforsite, intrusive into the Passo Feio Complex. The contacts relationships between alvikites and beforsites are too complex, therefore it is possible that they had occurred together and that the difference lied in the fluctuation of Mg activity in a calcitic magma.

(3) The shape of bodies observed in outcrops, drill cores and geophysical images indicates that they are tabular, like dikes or sills. Because of the shape of the bodies and no directly known igneous alkaline rock association, the carbonatites were classified as linear. In addition, the described porphyritic texture is indicative that they are shallow bodies. It might be a shallow expression of a larger body at depth.

(4) Calcite and dolomite followed by apatite are the dominant minerals in the Caçapava do Sul carbonatites, and constitute up to 80% of the rock. Biotite xenocrysts and hydrothermalized xenoliths of the biotite amphibolitic host rocks are abundant. Minerals containing REE are present in all carbonatite units and include monazite, pyrochlore-like minerals, bastnaesite, allanite and rontgenite. Zircon, baddeleyite, pyrite, rutile, chalcopyrite, barite, thorite and celestine are the other accessory minerals.

(5) The studied carbonatites have high CaO, P_2O_5, Nb and Sr. Trace element characteristics of alvikite and beforsite are similar and share the same ranges of abundances and distribution patterns with typical LREE enrichment.

(6) The Caçapava do Sul carbonatites lack alkalis, but the enrichment in one Passo Feio fenite suggests that the carbonatite magma contained Na but was relatively poor in K.
(7) The U-Pb zircon dating yielded an Ediacaran age for magmatism at ca. 603.2 ± 4.5 Ma, one of few Precambrian carbonatites in the Brazilian Shield, and the only dated carbonatite in southern Brazil related to the Pan-Gondwanaland (650–500 Ma) arc activity described by Veevers (2004, 2007).

Acknowledgments

This study is part of the Master of Science dissertation of Tiara Cerva-Alves at Programa de Pós-Graduação em Geociências, Universidade Federal do Rio Grande do Sul. The investigation was supported financially through a grant to Marcus V. D. Remus by Conselho Nacional do Desenvolvimento Científico e Tecnológico of Brazil (Exploração e origem de rochas fosfáticas e carbonáticas no RS: Novas fontes de insumos para a agricultura e indústria mineral – Edital Universal 14/2012, Proc. 482500/2012-3). We acknowledge the contributions of Alexandre R. da Rocha, Nilson Torres, Marcelo Gindri, Juliana Vargas, Francisco Benetti and Jhony de La Zerda, from Mining Ventures Brasil Group for carbonatite drill core samples, company data, field discussions and partnership, Gilberto Santos for guidance in laboratory procedures, Léo A. Hartmann and Karen Pires for incisive comments on this manuscript. We are grateful to an anonymous journal reviewer and Editor for contribution to the improvement of the article.

References

Adrião, A.B., 2015. Mantle heterogeneity on the source of Paraná continental flood basalt: new evidence from 128 Ma Rosário do Sul kimberlitic Province, Southern Brazil. Curso de Pós-Graduação em Geociências, Universidade Federal do Rio Grande do Sul, Porto Alegre, (Master's thesis) (unpublished). 45p.
Alkmim, F.F., 2004. O que faz de um cráton um cráton? O cráton do São Francisco e as revelações almedianas ao delimitá-lo. In: Mantesso-Neto, V., Bartorelli, A., Carneiro, C.D.R., Brito-Neves, B.B. (Eds.), Geologia do Continente Sul-Americano: Evolução da Obra de Fernando Flávio Marques de Almeida. Beca, São Paulo, pp. 17-35.
Almeida, F.F.M., 1967. Origem e evolução da Plataforma Brasileira. Boletim da Divisão de Geologia e Mineralogia. Departamento Nacional de Produção Mineral 241, 36 p.
Almeida, F.F.M., Hasui, Y., Brito Neves, B.B., Fuck, R.A., 1981. Brazilian structural provinces: an introduction. Earth Sci. Rev. 17 (1–2), 1–29.
Andrade, S., Ulbrich, H.H., Gomes, C.B., Martins, L., 2014. Methodology for the determination of trace and minor elements in minerals and fused rock glasses with laser ablation associated with quadrupole inductively coupled plasma mass spectrometry (LA-Q-ICPMS). Am. J. Anal. Chem. 5, 701–721.
Angélica, R.S., Costa, M.L., 1993. Geochemistry of rare-earth elements in surface lateritic rocks and soils from the Maicuru complex, Pará, Brazil. J. Geochem. Explor. 47, 165–182.
Antonini, P., Comin-Chiaramonti, P., Gomes, C.B., Censi, P., Riffel, B.F., Yamamoto, E., 2003. The Early Proterozoic carbonatite complex of Angico dos Dias, Bahia State, Brazil: geochemical and Sr-Nd isotopic evidence for a enriched mantle origin. Mineral. Mag. 67 (5), 1039–1057.
Barker, D.S., 1989. Field relations of carbonatites. In: Bell, K. (Ed.), Carbonatites: Genesis and Evolution. Unwin Hyman, London, pp. 38–69.
Barker, D.S., Nixon, P.G., 1989. High-Ca, low alkali carbonatite volcanism at Fort Portal, Uganda. Contrib. Miner. Petrol. 103, 166–177.
Belousova, E.A., Griffin, W.L., O'Reilly, S.Y., Fisher, N.I., 2002. Igneous zircon: trace element composition as an indicator of source rock type. Contrib. Miner. Petrol. 143, 602–622.
Biondi, J.C., 2005. Brazilian mineral deposits associated with alkaline and alkaline-carbonatite complexes. In: Comin-Chiaramonti, P., Gomes, C.B. (Eds.), Mesozoic to Cenozoic Alkaline Magmatism in the Brazilian Platform. Editora da Universidade de São Paulo/Fapesp, São Paulo, pp. 707–755.
Bitencourt, M.F., 1983. Geologia, petrologia e estrutura dos metamorfitos da região e Caçapava do Sul, RS. Curso de Pós-Graduação em Geociências, Universidade Federal do Rio Grande do Sul, Porto Alegre, (Master's thesis) (unpublished), 161 p.
Bitencourt, M.F., Florisbal, L.M., Sbaraini, S., Rivera, C.B., 2015. Idades U-Pb e a duração do magmatismo ultrapotássico do Maciço Sienítico Piquiri. Boletim de Resumos. IX Simpósio Sul-Brasileiro de Geologia. Florianópolis, SC. Brazil.
Burger Jr., C., Ribeiro, M., Gerhardt, A.L.B., 1988. On the alkaline rocks of Piratini, Rio Grande do Sul, Brazil. Paula-Coutiana 2, 81–112.
Caldasso, A.L., Sander, A., 1994. Diatrema de canguçu e Rochas Alcalinas Associadas. 38 Congresso Brasileiro de Geologia, Balneário Camburiú/SC. pp. 59–60.
Chakmouradian, A.R., Mumin, A.H., Demény, A., Elliott, B., 2008. Postorogenic carbonatites at Eden Lake, Trans-Hudson Orogen (northern Manitoba, Canada): Geological setting, mineralogy and geochemistry. Lithos 103, 503–526.
Chemale Jr., 2000. A Evolução Geológica do Escudo Sul-Rio-Grandense. In: Holz, M., De Ros, L.F. (Eds.), Geologia do Rio Grande do Sul. UFRGS, Porto Alegre, pp. 13–52.
Cordani, U.G., Brito-Neves, B.B., 1982. The geologic evolution of South America during the Archean and Early Proterozoic. Revista Brasileira de Geociências 12 (1–3), 78–88.
Corfu, F., Hanchar, J.M., Hoskin, P.W.O., Kinny, P., 2003. Atlas of Zircon Textures. In: Hanchar, J.M. and Hoskin, P.W.O (Eds), Zircon. Reviews in Mineralogy & Geochemistry 53, pp. 469–500.
Costa, M.L., Fonseca, L.R., Angélica, R.S., Lemos, V.P., Lemos, R.L., 1991. Geochemical exploration of the Maicuru alkaline-ultramafic-carbonatite complex, northern Brazil. J. Geochem. Explor. 40, 193–204.
Costanzo, A., Moore, K.R., Wall, F., Feely, M., 2006. Fluid inclusions in apatite from Jacupiranga calcite carbonatites: evidence for a fluid-stratified carbonatite magma chamber. Lithos 91, 208–228.
CPRM, 2010. Projeto Aerogeofísico Escudo Do Rio Grande Do Sul. LASA PROSPECÇÕES S.A./Geological Survey of Brazil, p. 260. Technical Report.
CPRM, 2015. Mapa Geológico Simplificado do Brasil. Geological Survey of Brazil, DGEO – Departamento de Geologia, DIGEOP – Divisão de Geoprocessamento, DIARMI – Divisão de Avaliação de Recursos Minerais.
Dalton, J.A., Wood, B.J., 1993. The compositions of primary carbonate melts and their evolution through wall rock reaction in the mantle. Earth Planet. Sci. Lett. 119, 511–525.
Dasgupta, R., Hirschmann, M.M., Dellas, N., 2004. The effect of bulk composition on the solidus of carbonated eclogite from partial melting experiments at 3 GPa. Contrib. Mineral. Petrol. 149, 288–305.
Doucelance, R., Hammouda, T., Moreira, M., Martins, J.C., 2010. Geochemical constraints on depth of origin of oceanic carbonatites: the Cape Verde case. Geochim. Cosmochim. Acta 74, 7261–7282.
Fragoso-Cesar, R. 1991. Tectônica de Placas no Ciclo Brasiliano: as orogenias dos cinturões Dom Feliciano e Ribeira no Rio Grande do Sul. Instituto de Geociências, Universidade de São Paulo, São Paulo, (Ph.D. thesis). 366p.
Fuck, E.A., Brito-Neves, B.B., Schobbenhaus, C., 2008. Rodinia descendants in South America. Precambr. Res. 160, 108–126.
Gastal, M.C.P., Lafon, J.M., Ferreira, J.F.F., Magro, J.F.U., Remus, M.V.D., Sommer, C.A., 2006. Reinterpretação do Complexo Intrusivo Lavas do Sul, RS, de acordo com os sistemas vulcano-plutônicos de subsidência. Parte 1: geologia, geofísica e geocronologia (207Pb/206Pb e 206Pb/238U). Revista Brasileira de Geociências 36 (1), 109–124.
Giovanini, A.L., 2013. Contribuição à geologia e geoquímica do carbonatito e da jazida (Nb, ETR) de Seis Lagos (Amazônia). Curso de Pós-Graduação em Geociências, Universidade Federal do Rio Grande do Sul, Porto Alegre, (Master's thesis) (unpublished), 128 p.
Gomes, C.B., Comin-Chiaramonti, P., 2005. An introduction to the alkaline and alkaline-carbonatitic magmatism in and around the Paraná Basin. In: Comin-Chiaramonti, P., Gomes, C.B. (Eds.), Mesozoic to Cenozoic Alkaline Magmatism in the Brazilian Platform. Editora da Universidade de São Paulo/Fapesp, São Paulo, pp. 21–29.
Gomes, C.B., Ruberti, E., Morbidelli, L., 1990. Carbonatite complexes from Brazil: a review. J. South Am. Earth Sci. 3 (1), 51–63.
Gomide, C.S., Brod, J.A., Vieira, L.C., Junqueira-Brod, T.C., Petrinovic, I.A., Santos, R.V., Barbosa, E.S.R., Mancini, L.H., 2016. Stable (C, O, S) isotopes and whole-rock geochemistry of carbonatites from Alto Paranaíba Igneous Province,SE Brazil. Brazilian J. Geol. 46 (3), 351–376.
Grazia, C.A., Toniolo, J.A., Parisi, G., Muller, E.L., Dressler, V.L., 2011. Prospecção hidrogeoquímica no carbonatito Três Estradas, RS. In: Congresso Brasileiro de Geoquímica, 13, Outubro, Gramado. Anais... Gramado, SBGq, pp. 1769-1772.
Hammouda, T., 2003. High pressure melting of carbonated eclogites experimental constraints on carbon recycling and storage in the mantle. Earth Planet. Sci. Lett. 214, 357–368.
Hammouda, T., Keshav, S., 2015. Melting in the mantle in the presence of carbon: review of experiments and discussion on the origin of carbonatites. Chem. Geol. 418, 171–188.
Hartmann, L.A., Remus, M.V.D., 2000. Origem e evolução das rochas ultramáficas do Rio Grande do Sul desde o Arqueano até o Cambriano. In: Holz, M., De Ros, L.F. (Eds.), Geologia do Rio Grande do Sul. CIGO/UFRGS, Porto Alegre, pp. 53–78.
Hartmann, L.A., Tindle, A., Bitencourt, M.F., 1990. O metamorfismo de fácies anfibolito no Complexo Passo Feio, RS com base em química dos minerais. Pesquisas 17 (12), 62–71.
Hartmann, L.A., Leite, J.A.D., da Silva, L.C., Remus, M.V.D., Mc-Naughton, N.J., Groves, D.I., Fletcher, I.R., Santos, J.O.S., Vasconcellos, M.A.Z., 2000. Advances in SHRIMP geochronology and their impact on understanding the tectonic and metallogenic evolution. Aust. J. Earth Sci. 47, 829–844.
Hartmann, L.A., Philipp, R.P., Santos, J.O.S., McNaughton, N.J., 2011. Time frame of 753–680 Ma juvenile accretion during the São Gabriel orogeny, southern Brazil. Gondwana Res. 19, 84–99.
Hoernle, K., Tilton, G., Le Bas, M.J., Duggen, S., Garbe-Schönberg, D., 2002. Geochemistry of oceanic carbonatites compared with continental

carbonatites: mantle recycling of oceanic crustal carbonate. Contrib. Miner. Petrol. 142, 520–542.
Hogarth, D.D., 1989. Pyrochlore, apatite and amphibole: distinctive minerals in carbonatite. In: Bell, K. (Ed.), Carbonatites: Genesis and Evolution. Unwin Hyman, London, pp. 149–176.
Hoskin, P.W.O., Ireland, T.R., 2000. Rare earth element chemistry of zircon and its use as a provenance indicator. Geology 28, 627–630.
Hou, Z., Tian, S., Yuan, Z., Xie, Y., Yin, S., Yi, L., Fei, H., Yang, Z., 2006. The Himalayan collision zone carbonatites in western Sichuan, SW China: Petrogenesis, mantle source and tectonic implication. Earth Planet. Sci. Lett. 244, 234–250.
Ignacio, C., Muños, M., Sagredo, J., 2012. Carbonatites and associated nephelinites from São Vicente, Cape Verde Islands. Mineral. Magazine 76 (2), 311–355.
Issler, R.S., Lima, M.I.C., Montalvão, M.B.G., Silva, G.G., 1975. Intrusivas feldspatoididas no Craton Guianes. Congresso Ibero-americano de Geologia Economica II, 363–382.
Jones, A.P., Genge, M., Carmody, L., 2013. Carbonate melts and carbonatites. Rev. Mineral. Geochem. 75, 289–322.
Kim, N., Cheong, A.C., Yi, K., Jeong, Y.-J., Koh, S.M., 2016. Post-collisional carbonatites-hosted rare earth element mineralization in the Hongcheon area, central Gyeonggi massif, Korea: ion microprobe monazite U-Th-Pb geochronology and Nd-Sr isotope geochemistry. Ore Geol. Rev. 79, 78–87.
Kiseeva, E.S., Yaxley, G.M., Hermann, J., Litasov, K.D., Rosenthal, A., Kamanetsky, V.S., 2012. An experimental study of carbonated eclogite at 3.5-5.5 GPa – implications for silicate and carbonate metasomatism in the cratonic mantle. J. Petrol. 53, 727–759.
Kjarsgaard, B.A., Hamilton, D.L., 1989. The genesis of carbonatites by immiscibility. In: Bell, K. (Ed.), Carbonatites: Genesis and Evolution. Unwin Hyman, London, pp. 388–404.
Lapin, A.V., Iwanuch, W., Ploshko, V.V.V., 1999. Carbonatitos Lineares de Cinturões Móveis: uma síntese. Revista Brasileira de Geociências 29 (4), 483–490.
Le Bas, M.J., 1989. Diversification of carbonatite. In: Bell, K. (Ed.), Carbonatites: Genesis and Evolution. Unwin Hyman, London, pp. 428–447.
Lemos, V.P., Costa, M.L., 1987. Partição dos Terras Raras nos Lateritos Fosfáticos de Maicuru – PA. 1 CBQq, 1, 83–102.
Lima, E.F., Nardi, L.V.S., 1998. The Lavras do Sul Shoshonitic Association: implications for the origin and evolution of Neoproterozoic shoshonitic magmatism in southernmost Brazil. J. S. Am. Earth Sci. 11 (1), 67–77.
Liz, J.D., Lima, E.F., Nardi, L.V.S., Sommer, C.A., Saldanha, D.L., Pierosan, R., Alexandre, F.M., 2005. Caracterização geológica e petrologia das rochas monzoníticas da Associação Shoshonítica de Lavas do Sul (RS). In: Simpósio sobre vulcanismo e ambientes associados. 3, Cabo Frio. Anais.
Lopes, C.G., Pimentel, M.M., Philipp, R.P., Gruber, L., Armstrong, R., Junges, S., 2015. Provenance of the Passo Feio complex, Dom Feliciano Belt: implications for the age of supracrustal rocks of São Gabriel Arc, southern Brazil. J. S. Am. Earth Sci. 58, 9–17.
Maciel, L.A.C., 2016. Rochas alcalinas no Rio Grande do Sul: controles tectônicos e mineralizações associadas. In: SIMEXMIN, Boletim de Resumos. Ouro Preto.
Mariano, A.N., 1989. Nature of economic mineralization in carbonatites and related rocks. In: Bell, K. (Ed.), Carbonatites: Genesis and Evolution. Unwin Hyman, London, pp. 149–176.
McDonough, W.F., Sun, S.S., 1995. The composition of the Earth. Chem. Geol. 67 (5), 1050–1056.
Mitchell, R.H., 2005. Carbonatites and carbonatites and carbonatites. Canadian Mineral. 43, 2049–2068.
Mitchell, R.H. 2005a. Mineralogical and Experimental Constraints on the Origin of Niobium Mineralization in Carbonatites. In: Linnen, R.L., Samson, I.M. (Eds.), Rare-Element Geochemistry and Mineral Deposits: Geological Association of Canada. GAC Short Course Notes, 17, 201–215.
Paim, P.S.G., Chemale Jr., F., Lopes, R.C., 2000. A Bacia do Camaquã. In: Holz, M., De Ros, L.F. (Eds.), Geologia do Rio Grande do Sul. UFRGS, Porto Alegre, pp. 231–274.
Parisi, G.N., Toniolo, J.A., Grazia, C.A., Pinto, L.G.R., 2010. Prospecção de fosfato no Rio Grande do Sul. In: Congresso Brasileiro de Geologia, 30, Belém do Pará. AnaisEllipsis Belém do Pará, SBG, 236 pp.
Philipp, R.P., Vieiro, A.P., Comin-Chiaramonti, P., Gomes, C.B., 2006. Mesozoic Alkaline Rocks of Rio Grande do Sul. In: Comin-Chiaramonti, P., Gomes, C.B. (Eds.), Mesozoic to Cenozoic Alkaline Magmatism in the Brazilian Platform. Editora da Universidade de São Paulo/Fapesp, São Paulo, pp. 573–590.
Philipp, R.P., Pimentel, M.M., Chemale Jr., F., 2016. Tectonic evolution of the Dom Feliciano Belt in southern Brazil: Geological relationships and U-Pb geochronology. Brazilian J. Geol. 46 (Suppl. 1), 83–104.
Pinto, V.M., Hartmann, L.A., Santos, J.O.S., McNaughton, N.J., Wildner, W., 2011. Zircon U-Pb geochronology from the Paraná bimodal volcanic province suport a brief eruptive cycle at ~135 Ma. Chem. Geol. 281, 93–102.
Remus, M.D.V., Hartmann, L.A., McNaughton, M.J., Fletcher, I.R., 1999. Shrimp U-Pb zircon ages of volcanism from São Gabriel Block, southern Brazil. In: Simpósio sobre vulcanismo e ambientes associados. 1. Boletim de Resumos. 83 pp.
Remus, M.V.D., Hartmann, L.A., McNaughton, M.J., Groves, D.I., Reischl, J.L., 2000. Distal Magmatic-Hydrothermal Origin for the Camaquã Cu (Au-Ag) and Santa Maria Pb, Zn (Cu-Ag) Deposits, Southern Brazil. Gondwana Res. 3 (2), 155–174.
Ribeiro, M., Bocchi, P.R., Figueiredo Filho, P.M., Tessari, R.I., 1966. Geologia da quadrícula de Caçapava do Sul, RS, Brasil. Boletim da Divisão de Geologia e Mineralogia, DPM-DNPM, pp. 127-232.
Riccomini, C., Velázquez, V.F., Gomes, C.B., 2005. Tectonic controls of the Mesozoic and Cenozoic alkaline magmatis in the central-southeastern Brazil Platform. In: Comin-Chiaramonti, P., Gomes, C.B. (Eds.), Mesozoic to Cenozoic Alkaline Magmatism in the Brazilian Platform. Editora da Universidade de São Paulo/Fapesp, São Paulo, pp. 31–56.
Rocha, A.M.R., Dorneles, N.T., Gindri, M.D., Vargas, F.M., Cerva-Alves, T., Benetti, F.A., 2013. Descoberta dos carbonatitos Picada dos Tocos e Passo Feio e o potencial para fosfato e ETRs, Caçapava do Sul, Rio Grande do Sul. In: III Brazilian Symposium of Metallogeny – The New Brazilian Mineral Deposits. Gramado/Rio Grande do Sul. Boletim de Resumos.
Saalmann, K., Gerdes, A., Lahaye, Y., Hartmann, L.A., Remus, M.V.D., Laufer, A., 2010. Multiple accretion at the eastern margin of the Rio de La Plata craton, the prolonged Brasiliano orogeny in southernmost Brazil. Int. J. Earth Sci. 100, 355–378.
Silva, A.B., Liberal, G.S., Grossi Sad, J.H., Issa Filho, A., Rodrigues, C.S., Riffel, B.F., 1988. Geologia e petrologia do complexo Angico dos Dias (Bahia, Brasil), uma associação carbonatítica Precambriana. Geochimica Brasiliensis 2, 81–108.
Silva, L.C., McNaughton, N.J., Armstrong, R., Hartmann, L.A., Fletcher, I.R., 2005. The Neoproterozoic Mantiqueira Province and its African connections: a zircon-based U-Pb geochronologic subdivision for the Brasiliano/Pan-African system of orogens. Precambr. Res. 136, 203–240.
Sommer, C.A., Lima, E.F., Nardi, L.V.S., Figueiredo, A.M.G., Pierosan, R., 2005. Potassic and low- and high-Ti mildly alkaline volcanism in the Neoproterozoic Ramada Plateau, southernmost Brazil. J. S. Am. Earth Sci. 18, 237–254.
Sommer, C.A., Lima, E.F., Nardi, L.V.S., Liz, J.D., Waichel, B.L., 2006. The evolution of Neoproterozoic magmatism in Southernmost Brazil: shoshonitic, high-K tholeiitic and silica-saturated, sodic alkaline volcanism in post-collisional basins. Ann. Brazilian Acad. Sci. 78 (3), 573–589.
Svisero, D.P., Chieregati, L.A., 1991. Contexto geológico de kimberlitos, lamproítos e ocorrências diamantíferas do Brasil. Boletim IG-USP (Série Científica) 9 (9), 75–81.
Tedesco, M.A., Robaina, L.E.S., 1991. Caracterização geoquímica de piroxênios e granadas da brecha kimberlítica de São Vicente, RS. In: Congresso Brasileiro de Geoquímica, 3; Congresso de Geoquímica dos Países de Língua Portuguesa, 1, São Paulo. Brasil. Anais, 1, 707–710.
Thomsen, T.B., Schmidt, M.W., 2008. Melting of carbonated pelites at 2.5-5.0 GPa, silicate-carbonatite liquid immiscibility, and potassium-carbon metasomatism of the mantle. Earth Planet. Sci. Lett. 267, 17–31.
Toniolo, J.A., Parisi, G.N., Grazia, C.A., Reischl, J.L., 2010. Prospecção de fosfato na área de Três Estradas, Lavras do Sul, RS. In: Simpósio Brasileiro de Exploração Mineral, 4, Ouro Preto. Ouro Preto, ADIMB.
Toniolo, J.A., Remus, M.V.D., Parisi, G.N., Dani, N., 2013. Dois eventos carbonatíticos temporalmente distintos no RS: tipos linear e central. VIII Simpósio Sulbrasileiro de Geologia, FIERGS, 21-24 de julho de 2013. Porto Alegre, RS, Resumos.
Veevers, J.J., 2004. Gondwanaland from 650–500 Ma assembly through 320 Ma merger in Pangea to 185–100 Ma breakup: supercontinental tectonics via stratigraphy and radiometric dating. Earth Sci. Rev. 68, 1–132.
Veevers, J.J., 2007. Pan-Gondwanaland post-collisional extension marked by 650–500 Ma alkaline rocks and carbonatites and related detrital zircons: a review. Earth Sci. Rev. 83, 1–47.
Winter, J.D., 2010. Principles of Igneous and Metamorphic Petrology. second ed. Prentice Hall Ed., 720 pp.
Woodard, J., Hetherington, C.J., 2014. Carbonatite in a post-collisional tectonic setting: geochronology and emplacement conditions at Naantali, SW Finland. Precambr. Res. 240, 94–107.
Woodard, J., Hölttä, P., 2005. The Naantali alvikite vein-dikes: a new carbonatite in southwestern Finland. Geol. Surv. Finland Spec. Pap. 38, 5–10.
Woolley, A.R., 2003. Igneous silicate rocks associated with carbonatites: their diversity, relative abundances and implications for carbonatite genesis. Periodico di Mineralogia 72, 9–17.
Woolley, A.R., Kempe, D.R.C., 1989. Carbonatites: nomenclature, average chemical compositions, and element distribution. In: Bell, K. (Ed.), Carbonatites: Genesis and Evolution. Unwin Hyman, London, pp. 1–14.
Wyllie, P.J., 1989. Origin of carbonatite: evidence from phase equilibrium studies. In: Bell, K. (Ed.), Carbonatites: Genesis and Evolution. Unwin Hyman, London, pp. 500–545.
Wyllie, P.J., Lee, W.-J., 1998. Model system controls on conditions for formation of magnesiocarbonatite and calciocarbonatite magmas from mantle. J. Petrol. 39, 1885–1893.
Yaxley, G.M., Brey, G.P., 2004. Phase relations of carbonate-bearing eclogite assemblages from 2.5 to 5.5 GPa: implications for petrogenesis of carbonatites. Contrib. Miner. Petrol. 146, 606–619.